9 420278

Pressure Sensitive Paints

(Review article submitted for *Experiments in Fluids*)

Tianshu Liu†, T. Bencic‡ and J. P. Sullivan*

† High Technology Corporation
28 Research Drive, Hampton, VA 23666
e-mail: tianshu@htc-tech.com
Tel.: (757) 865-0818 and Fax: (757) 865-6766

‡ NASA Glenn Research Center
21000 Brookpark Rd, MS 77-1
Cleveland, OH 44135
e-mail: timthy.j.bencic@lerc.nasa.gov
Tel: (216) 433-5690 and Fax: (216) 433-8643

* School of Aeronautics and Astronautics
Purdue University, West Lafayette, IN 47906
e-mail: sulivan@ecn.purdue.edu
Tel: (317) 494-3348 and Fax: (317) 494-0307

Abstract

This article reviews new advances and applications of pressure sensitive paints in aerodynamic testing. Emphasis is placed on important technical aspects of pressure sensitive paint including instrumentation, data processing, and uncertainty analysis.

1. Introduction

Pressure sensitive paint (PSP) has been developed for measuring air pressure on a surface based on oxygen quenching of luminescence. Unlike conventional techniques such as pressure taps, PSP is a global surface pressure measurement technique with high spatial resolution and good accuracy. Peterson and Fitzgerald (1980) demonstrated a surface flow visualization technique based on oxygen quenching of dye fluorescence and revealed the possibility of using an oxygen quenching sensor for surface pressure measurement. The Central Aero-Hydrodynamic Institute (TsAGI) in Russia pioneered PSP applications in aerodynamic testing (Ardasheva et al. 1985, Volan and Alati 1991, Bukov et al. 1992, Bukov et al. 1993, Troyanovsky et al. 1993). In the United States, PSP was developed independently by Gouterman's group at the University of Washington (Gouterman et al. 1990, Kavandi et al. 1990). Their paints have been used at NASA Ames (McLachlan et al. 1993, 1995a, 1995b, Bell and McLachlan 1993) and the Boeing Company. Considerable work on PSP has also been done at McDonnell Douglas (Morris et al. 1993a, 1993b, 1995, Donovan et al. 1993, Dowgwillo, et al. 1994, Crites 1993). Now, PSP has been commonly used in wind tunnel tests in major aerospace institutions throughout the world and applied to a variety of problems in aerodynamics. Useful reviews on PSP were previously given by Crites (1993), McLachlan and Bell (1995a), Liu

et al. (1997a), and Mosharov et al. (1997). This article reviews the latest development in PSP and discusses some important technical issues in instrumentation, data processing and uncertainty analysis.

2. PSP Fundamentals

Luminescence is a radiative phenomenon that occurs when a molecule is excited by a light with a proper wavelength. After electrons in a molecule are excited to a higher energy level from the ground state, the excited state returns to the ground state through emission of a photon (radiative decay) or non-radiative decay. The non-radiative process relevant to PSP is oxygen quenching in which the excited state is deactivated by interaction with oxygen. The oxygen quenching competes with depopulation of the excited state by luminescence. As a result, the higher amount of oxygen reduces the luminescent emission intensity. This is the physical foundation for the use of PSP in aerodynamic testing since air pressure is proportional to oxygen partial pressure. More detailed discussions of the underlying photophysical processes in PSP were given by Gouterman (1997).

The quantum yield $\ddot{O}$ of the luminescent emission in the presence of an oxygen quencher is described by

$$\ddot{O} = \frac{I}{I_a} = \frac{k_r}{k_r + k_{nr} + k_q[O_2]} = k_r \hat{o} \qquad (1)$$

where I is the luminescence intensity, I_a is the absorption intensity, k_r is the rate constant for radiative decay, k_{nr} is the rate constant for non-radiative deactivation, k_q is the rate constant for oxygen quenching, $[O_2]$ is the concentration of oxygen, and τ is the lifetime

of an excited molecule. Dividing (1) into the quantum yield in the absence of oxygen and considering $[O_2] \propto P$, one can obtain a generic form of the Stern-Volmer equation

$$\frac{I_0}{I} = \frac{\hat{o}_0}{\hat{o}} = 1 + KP \tag{2}$$

where K is the Stern-Volmer coefficient, I_0 is the luminescent intensity in the absence of oxygen, and P is the air pressure. The Stern-Volmer equation provides a basic relation between air pressure and luminescent intensity or lifetime.

The Stern-Volmer coefficient is temperature-dependent and temperature variation is one of major error sources in PSP measurement. Temperature affects two physical processes: non-radiative deactivation and oxygen diffusion in a polymer. The deactivation term k_{nr} can be decomposed into a temperature-independent part k_{nr0} and a temperature-dependent part k_{nrl}. The rate k_{nrl} has the Arrhenius form $k_{nrl} \propto exp(-E_{nr}/RT)$, where E is the Arrhenius activation energy, R is the universal gas constant, and T is the thermodynamic temperature (in Kelvin) (Bennett and McCartin 1966, Song and Fayer 1991). The temperature dependence of the non-radiative process is intrinsic for PSP. On the other hand, temperature can also affect oxygen diffusion in a polymer. For a diffusion-limited quenching reaction, the quenching rate constant k_q is described by the Smoluchowski equation $k_q = 4\eth N p(D_p + D_q)$, where D_p and D_q are the diffusion coefficients of the probe and quencher in the polymer, N is the number of molecules per millimole and p is a factor that depends on the quenching mechanism (Szmacinski and Lakowicz 1995). Over a temperature range, the diffusion coefficients are related to temperature in the Arrhenius form like $D_q \propto exp(-E_q/RT)$, where E_q is the activation energy for the diffusion process of the quencher $[O_2]$. A question related to the design of

PSP formulations is which mechanisms dominate the temperature dependence of a PSP. Experiments (Gewehr and Delpy 1993, Schanze et al. 1997) for two different paints indicate that the temperature dependence of the oxygen diffusivity in the polymer dominates the temperature dependence of PSP. This finding has important implications for the design of low-temperature-sensitive PSP formulations. The low-temperature-sensitive PSP has a polymer binder with low activation energy for diffusion of oxygen.

3. Paint Formulations

Generally, PSP have two ingredients: probe luminescent molecule and polymer binder. The polymer binder serves as a matrix where the probe molecules are immobilized and an anchor to adhere PSP to a surface. Selection of a good paint formulation is a key for PSP measurement. A well-known PSP formulation is Platinum octaethylporphyrin (PtOEP) in GP-197 dimethylsiloxane polymer invented by Gouterman's group at the University of Washington (McLachlan et al. 1993). Another known formulation is Bathophenanthroline Ruthenium in GE RTV 118 silicone polymer used by McDonnell Douglas group (Sacksteder et al. 1993). Moshasrov et al. (1997) have described the properties of PSPs developed by TsAGI. and listed some luminophores for oxygen sensors such as Pyrene and Platinum group metal complexes. Some PSP formulations have been also summarized by Liu et al. (1997a), while many formulations are proprietary. Figure 1 shows typical calibration results of luminescent intensity and phase at different temperatures for PtTFPP adsorbed onto a tape made of a polymer/ceramic composite composed of aluminum oxide particles and about 25% volume of a poly(acrylic) binder.

Figure 2 shows calibration results of intensity and phase at different temperatures for Bathophen Ruthenium Chloride in RTV 110 and Silica Gel.

Recent attempts are made on the development of multiple-luminophore PSP, cryogenic PSP, low-temperature-sensitive PSP, and fast time-responding PSP. Several formulations of dual-luminophore PSP have been suggested by Oglesby et al. (1995b, 1996), and Harris and Gouterman (1998). Cryogenic PSP is needed for global pressure measurements in cryogenic wind tunnels such as the National Transonic Facility at NASA Langley. The cryogenic PSP must work in near-zero-oxygen and cryogenic temperature conditions since the working gas is pure nitrogen and temperature is from 90 to 170 Kelvins in cryogenic wind tunnels. Asai et al. (1997) first developed a matrix-free PSP coating on an anodized aluminum surface and obtained the surface pressure distributions on a model in a cryogenic wind tunnel. Upchurch et al. (1998) developed a polymer-based cryogenic PSP that is universally applicable to all types of surfaces such as stainless steel. A temperature insensitive PSP would be good since the temperature dependence of PSP introduces significant error in pressure measurement. However, the development of this kind of paint is a difficult task because luminescence is intrinsically dependent of temperature (Schanze et al. 1997). Puklin et al. (1998) studied a PSP formulation based on a fluoroacrylic polymer called FIB. This paint exhibits the low temperature dependence since FIB has extraordinarily low activation energy for diffusion of oxygen. It is noted that two TsAGI's PSP formulations based on silicone rubber and some derivative of pyren as a luminophore have low temperature sensitivity over a temperature range from –20 to 40 °C (Moshasrov et al. 1997).

Several fast-responding PSPs were tested by Baron et al. (1993). The time response of PSP is limited by the diffusion process of oxygen through the polymer layer and can be improved by increasing the gas permeability of the polymer. Recently, Ponomarev and Gouterman (1998) found that the better time response can be achieved by adding an appropriate amount of hard pigment particles into PSP. When the pigment volume concentration exceeds a critical level, the response time of the PSP is dramatically reduced and the smallest response time is 0.5 ms. Sol-Gel-Based PSP developed by Jordan et al. (1999) can also achieve a response time of the order of milliseconds.

4. Measurement Systems

Hardware of a PSP measurement system includes paint, illumination light source, optical filter, photodetector, and computer. From the viewpoint of instrumentation, there are two kinds of systems for PSP: intensity-based system and lifetime-based system. The intensity-based system with a scientific-grade CCD camera is the mostly used in PSP measurements, while the lifetime-based techniques are being rapidly developed. Each system has its advantages over the others in certain areas and also particular problems associated with it. Typical intensity-based systems are CCD camera systems for single-luminophore and dual-luminophore PSPs. Luminescent lifetime measurements are usually made using a laser-scanning system and a lifetime imaging system. The instrumentation and data reduction procedure are different for the intensity-based and lifetime-based systems.

4.1. Intensity-based systems

Single-luminophore PSP

The intensity-based system with a CCD camera for a single-luminophore PSP is shown in Figure 3. PSP is applied to a model surface. The paint is excited by an illumination source with an appropriate wavelength. A CCD camera detects luminescent emission from the PSP layer, which is filtered optically to eliminate the illumination light before entering the camera. The luminescent image is digitized for data processing. Selection of an illumination source depends on the absorption spectrum of the paint. The source must provide a large number of photons in a wavelength band of the absorption spectrum. A variety of illumination sources are available, which include lasers (Morris et al. 1993b, Crites 1993), xenon lamps (McLachlan et al. 1993), tungsten/halogen lamps (Dowgwillo et al. 1994), and array of blue light-emitting diodes (LED) (Clinehens and Dale 1998). Morris et al. (1993a) and Crites (1993) discussed the characteristics of some illumination sources. Scientific grade cooled CCD digital cameras are used for luminescence measurement. These cameras can provide high intensity resolution (12 to 16 bits) and high spatial resolution (up to 2048×2048 pixels). They also exhibit good linearity and high signal-to-noise ratio (SNR).

In order to eliminate effects of spatial non-uniformities of illumination intensity, paint thickness, and luminophore concentration, one must take a ratio between a wind-on image and a wind-off image at a known constant reference pressure P_{ref}. Thus, the Stern-Volmer relation has the following form for data reduction,

$$\frac{I_{ref}}{I} = A(T) + B(T)\frac{P}{P_{ref}}. \tag{3}$$

In some cases, a higher-order polynomial form of (3) is used to take non-linear effects into account. Theoretically, it is straightforward to calculate air pressure from the intensity ratio as long as the Stern-Volmer coefficients *A(T)* and *B(T)* are determined by paint calibration. However, since aerodynamic forces may produce model deformation in wind tunnel tests, the wind-on image does not align with the wind-off image. Thus, direct pixel-to-pixel image ratioing fails. The ratio between two non-aligned images leads to considerable errors in calculating pressure such that some distinct flow features like shocks could be smeared. In order to correct this misalignment, image registration must be used before image ratioing (Bell and McLachlan 1993 and Donovan et al. 1993). Model deformation significantly complicates data reduction procedure. The wind-on and wind-off images are read and dark current images are subtracted from both images. Next, the images are divided by flat-field images to eliminate the pattern noise of the CCD camera. The wind-on image is realigned to the wind-off image through image registration. At this stage, the realigned wind-on and wind-off images are ready for pixel-to-pixel ratioing and the resulting intensity ratio image is converted to a pressure image using the Stern-Volmer relation. The final step is to map pressure data in two-dimensional (2D) image plane onto a surface grid in three-dimensional (3D) object space.

Dual-luminophore PSP

The purposes of developing dual-luminophore PSPs are twofold (Oglesby et al. 1995b, 1996, Harris and Gouterman 1995, Lyonnet et al. 1997, Bykov, et al. 1997). First, the use of a dual-luminophore PSP may eliminate the need of a wind-off reference image if the PSP consists of a pressure-sensitive luminophore with a pressure-insensitive reference luminophore. Secondly, a dual-luminophore PSP is used for temperature correction in

PSP measurements when a temperature sensitive luminophore that is not quenched by oxygen is combined with an oxygen sensitive luminophore. The probe luminophore and reference luminophore should have a common region in the absorption spectra and they can be excited by the same illumination light. Also, they should have non-overlapped emission spectra such that luminescent emissions from different luminophores can be completely separated by optical filters. Ideally, the ratio between these two-color images can eliminate the effect of spatial non-uniformity in illumination. Particularly, when two luminophores have comparable temperature sensitivities, the two-color ratio reduces the temperature effect on PSP measurement (Lyonnet et al. 1997). The dependence of the two-color intensity ratio $I_{\lambda_1} / I_{\lambda_2}$ on pressure P and temperature T is generally expressed as

$$I_{\lambda_1} / I_{\lambda_2} = F(P, T).$$

The CCD camera system for a single-luminophore PSP can be adapted for a dual-luminophore PSP when the optical filters is switched to take two-color images during a test. Some experiments indicate that a dual-luminophore PSP can correct variations in illumination intensity (Oglesby et al. 1995b, Harris and Gouterman 1995). Three pressure sensitive paints with an internal temperature sensitive luminophore have also been tested by Oglesby et al. (1996). Torgerson et al. (1996) used a dual-luminophore PSP to measure the surface pressure distribution in a low speed impinging jet. They found that the simple two-color intensity ratio $I_{\lambda_1} / I_{\lambda_2}$ cannot eliminate the effect of dye concentration because two luminophores cannot be perfectly mixed. In this case, a ratio

of ratios $(I_{\lambda_1}/I_{\lambda_2})/(I_{\lambda_1}/I_{\lambda_2})_0$ should be used, where the subscript '0' denotes the wind-off condition. Hence, the calibration relation is modified as

$$(I_{\lambda_1}/I_{\lambda_2})/(I_{\lambda_1}/I_{\lambda_2})_0 = F(P,T).$$

From a theoretical model of paint-system response, McLean (1998) analyzed the sufficient conditions for the use of the simple ratio $I_{\lambda_1}/I_{\lambda_2}$ and the ratio of ratios $(I_{\lambda_1}/I_{\lambda_2})/(I_{\lambda_1}/I_{\lambda_2})_0$ to correct the spatial variations of paint properties. He pointed out that the ratio of ratios is necessary to correct for non-homogenous dye concentration and paint-thickness variation if a broadband illumination source is used. Although the ratio of ratios still needs the wind-off images, the image registration is not absolutely required.

4.2. Lifetime-based systems

Laser scanning system

Generally speaking, the lifetime method is based on measuring a response of PSP to an external time-varying excitation. The response of luminescence intensity I to an external forcing $F(t)$ is described as a first-order system

$$dI/dt = -I/\hat{o} + F(t), \tag{4}$$

where $\hat{o}$ is the luminescent lifetime. For a pulse laser with $F(t) = \ddot{a}(t)$, the luminescent response is simply an exponential decay

$$I = exp(-t/\hat{o}). \tag{5}$$

For a sinusoidally-modulated excitation $F(t) = 1 + H\,sin(\grave{u}\,t)$, the luminescence response after a short transient process is

$$I = \hat{o}[\,1 + H(1 + \hat{o}^2\grave{u}^{\,2})^{-1/2}\,sin(\grave{u}\,t - \ddot{o})\,], \tag{6}$$

where the phase angle $\ddot{o}$ is related to the luminescent lifetime, $tan\ddot{o} = \grave{u}\ \hat{o}$. For a micro-heterogeneous PSP that has multiple luminescent lifetimes, a high-order model is needed. Nevertheless, the response of PSP in a high-order model is qualitatively similar to the first-order model. Since the luminescent lifetime also obeys the Stern-Volmer relation (Eq. 2), one can obtain pressure by measuring either the lifetime $\hat{o}$ or phase angle $\ddot{o}$. Compared with the intensity-based method, the greatest advantage of the lifetime method is that the lifetime-pressure relation is not dependent on illumination. Therefore, the problem of non-uniformity in illumination becomes essentially irrelevant to the lifetime system. In addition, the lifetime measurement is insensitive to luminophore concentration, paint thickness, photodegradation, and paint contamination.

Figure 4 shows a generic laser scanning lifetime system for PSP. A low-power laser is modulated at a given frequency, focused to a small point and scanned over a model surface using a computer-controlled 2D scanner. The modulated laser excites the paint on the model surface and the responding luminescence is detected by a low noise photodetector (e.g. a PMT). The phase angle between the excitation and luminescent emission is obtained by using a lock-in amplifier, and the signal is digitized with a high resolution A/D converter and processed to obtain pressure. The scanner is synchronized to the data acquisition so that the position of the laser spot on the model is accurately known. The laser scanning system can simultaneously detect both the luminescent intensity and phase angle. Torgerson et al. (1996) used the laser scanning system to measure the surface pressure distributions in a low-speed impinging jet and on an airfoil in a transonic wind tunnel. This system was further refined by Lachendro et al. (1998) and recently used to measure the pressure distributions on a wing of a Beechjet 400A aircraft

in flight. Davies et al. (1995) developed a lifetime-based system with a pulse laser to directly determine the lifetime. Using this system, they measured the pressure distributions on a cylinder in subsonic flow and on a wedge at Mach 2. Note that the intensity-based laser scanning system has been used by Hamner et al. (1994), and Burns and Sullivan (1995).

Lifetime imaging system

A promising lifetime-based technique for PSP is the fluorescent lifetime imaging (FLIM) system that was originally developed by biochemists for oxygen detection in a small area (Hartmann and Ziegler 1996, Szmacinski and Lakowicz 1995). Unlike the laser scanning system, the FLIM system is a full-field lifetime measurement system. Recently, a practical FLIM system for PSP measurement in wind tunnels has been developed and tested in Defence Evaluation and Research Agency (DERA) in England (Holmes, 1998). The DERA's FLIM system comprises a solid-state, phase-sensitive camera, modulated blue LED array, associated control hardware and computer. The phase-sensitive camera and modulated excitation light are two key components in the FLIM system. The working principles and architecture of a phase-sensitive CCD camera were described by Fisher et al. (1999). When the modulated excitation light is $F(t) = 1 + H \sin(\omega t)$, the phase-sensitive camera provides two images integrated over a gate time form 0 to $1/2f$ (0 to π in ωt) and another gate time from $1/2f$ to $1/f$ (π to 2π in ωt), respectively. From the luminescent response (6), one obtains the ratio of these gated images as a function of the lifetime

$$I_2/I_1 = \int_{1/2f}^{1/f} I\,dt \Big/ \int_0^{1/2f} I\,dt = \frac{\delta(1+\omega^2\delta^2) - 2H}{\delta(1+\omega^2\delta^2) + 2H}. \qquad (7)$$

Obviously, the ratio of these images only depends on the lifetime and therefore is related to air pressure for a fixed modulation frequency. The FLIM system has the same advantages as other lifetime methods.

5. Data Analysis Techniques

Data reduction for PSP involves several data analysis problems. For a CCD camera system with a single-luminophore PSP, a deformed wind-on image must be re-aligned with a wind-off image through a mathematical transformation. This procedure is known as image registration. Another major problem is mapping pressure data in 2D image plane onto a model surface in 3D object space. This problem is related to camera calibration by solving the collinearity equations in photogrammetry.

5.1. Image Registration

The intensity-based method needs to take a ratio between a wind-on image and a wind-off image at a known reference pressure. Since a model may deform due to aerodynamic loads, the wind-on image does not align with the wind-off one. In order to solve this misalignment problem, image registration was suggested by Bell and McLachlan (1993) and Donovan et al. (1993). The image registration is based on a mathematical transform that maps the distorted wind-on image coordinates *(x', y')* onto the reference wind-off image coordinates *(x, y)*. In general, the transform can be expressed as polynomials

$$(x, y) = (\sum_{i,j=0}^{m} a_{ij} x'^{i} y'^{j} , \sum_{i,j=0}^{m} b_{ij} x'^{i} y'^{j}). \tag{8}$$

Geometrically, the constant terms represent translation, the linear terms represent rotation, shearing and stretching, and the non-linear terms represent higher-order corrections. To determine the unknown coefficients a_{ij} and b_{ij}, black fiducial marks are placed on the model. The number of the marks needed depends on how many unknown coefficients are to be determined. For a sufficient number of the marks, these coefficients can be obtained by solving a least-squares problem to match the coordinates of the marks in the wind-on and wind-off images. In general, the second-order polynomials ($m = 2$) can achieve adequate accuracy in the image registration. Recently, Weaver et al. (1999) utilized spatial anomalies (dots formed from aerosol mists in spraying) in a base coat and calculated a pixel shift vector field by using a spatial correlation technique. Based on the shift vector field, the wind-on image is registered. Le Sant et al. (1997) also described an automatic scheme for target recognition and image alignment. As a pure geometric method, however, the image registration cannot correct a change in illumination intensity on a model surface caused by movement of the model relative to the light sources. The error induced by the illumination variation on the surface due to the model movement may be significant for large deformation in a non-homogenous illumination field (Bell and McLachlan 1993). This problem actually provokes the development of the dual-luminophore PSP and lifetime imaging techniques that do not relied on the image registration.

5.2. Camera calibration and pressure mapping

Just like any other image-based measurement techniques, PSP extracts data from 2D image and maps them onto a surface in 3D object space. Photogrammetry provides a relationship between 3D coordinates in object space and corresponding 2D coordinates in

images (Wong 1980, McGlone 1989). A key photogrammetric problem is camera calibration which determines the camera orientation parameters and additional parameters in the collinearity equations relating 2D image plane to 3D object space. The collinearity equations relating a point (X, Y, Z) in object space to the corresponding point (x, y) in the image plane are

$$x - x_p + dx = -c\frac{m_{11}(X - X_c) + m_{12}(Y - Y_c) + m_{13}(Z - Z_c)}{m_{31}(X - X_c) + m_{32}(Y - Y_c) + m_{33}(Z - Z_c)},$$
$$y - y_p + dy = -c\frac{m_{21}(X - X_c) + m_{22}(Y - Y_c) + m_{23}(Z - Z_c)}{m_{31}(X - X_c) + m_{32}(Y - Y_c) + m_{33}(Z - Z_c)}. \quad (9)$$

In (9), a parameter set (c, x_p, y_p) is the interior orientation of a camera, where c is the principal distance of the lens, x_p and y_p are the principal-point coordinates on the image plane. Another parameter set $(\omega, \phi, \kappa, X_c, Y_c, Z_c)$ is the exterior orientation of a camera, where (ω, ϕ, κ) are the rotational angles and (X_c, Y_c, Z_c) are the coordinates of the perspective center in object space. The coefficients m_{ij} $(i, j = 1, 2, 3)$ are the rotation matrix elements that are functions of (ω, ϕ, κ) (McGlone 1989). The terms dx and dy are the image coordinate shifts induced by lens distortion. The models for the lens distortion terms are related to the additional parameters such as the radial and decentering distortion parameters, and the CCD pixel ratio (Fraser 1992, Fryer 1989). Analytical camera calibration techniques are needed to solve the collinearity equations (9) for determination of the interior and exterior orientation parameters and additional parameters of a camera/lens system. The bundle adjustment method, an iterative least-squares estimation method, has been used as a standard technique for the solution of the collinearity

equations in photogrammetry (Wong 1980, McGlone 1989). However, there is a singularity problem in inversion of an ill-conditioned normal equation matrix, which mainly results from strong correlation between the exterior and interior orientation parameters. In order to reduce the singularity, it is required to use multiple camera stations, varying image scales, different camera roll angles and a well-distributed target field in three dimensions (Fraser 1989, 1992). Obviously, these procedures in the bundle adjustment are not practical for on-site camera calibration in wind tunnels where optical access is limited and preparation time is short. For PSP applications in wind tunnels, a single-image method of on-the-job camera calibration is desirable that is simple to implement and less time consuming in order to have a minimum impact on productivity of wind tunnels.

Current PSP data reduction software uses simple methods such as image resection (Donovan et al. 1993, Le Sant and Merienne 1995) and Direct Linear Transformation (DLT) (Bell and McLachlan 1993). The resection method determines the camera exterior orientation parameters by assuming that the interior orientation and additional parameters are known. For a non-calibrated camera/lens system, the use of the resection method may cause considerable residual in least-square estimation if the interior orientation and additional parameters are not given appropriately. DLT, originally proposed by Abdel-Aziz and Karara (1971), is a clever method to solve the collinearity equations without the lens distortion. The DLT equations can be obtained by rearranging the collinearity equations, that is,

$$x + dx = \frac{L_1 X + L_2 Y + L_3 Z + L_4}{L_9 X + L_{10} Y + L_{11} Z + 1}$$
$$y + dy = \frac{L_5 X + L_6 Y + L_7 Z + L_8}{L_9 X + L_{10} Y + L_{11} Z + 1} \quad (10)$$

where L_k ($k = 1$ *to* 11) are the DLT parameters which are related to the camera orientation parameters. When the lens distortion terms dx and dy are neglected, the DLT equations are linear for the DLT parameters and can be solved directly using linear least-squares method without an initial guess. Because of its simplicity, DLT is widely used in close-range photogrammetry and machine vision. However, DLT gives poor estimates for the principal-point location and has large residual in least-squares estimation when the lens distortion exists. To take the lens distortion into account, iterative solution method has to be used such that DLT loses the simplicity. In spite of above demerits, DLT is still useful since it offers initial approximations for other more accurate methods. Recently, an optimization method for camera calibration has been developed by Liu *et al.* (1999a) and it has been used in a videogrammetric model deformation system. To avoid the singularity problem in solving the collinearity equations, this method uses two separate, but interacting procedures: resection for the exterior orientation parameters and optimization for the interior orientation and additional parameters. The optimization problem is suitably formulated based on the invariant property of the collinearity equations. The optimization method can obtain the exterior orientation, interior orientation and additional parameters from a single image of a calibration target plate with reasonable accuracy. Combined with DLT, the optimization method allows automatic camera calibration

without an initial guess of the orientation parameters. This feature particularly facilitates PSP measurements in wind tunnels.

After the camera orientation parameters are determined, PSP data can be mapped from a pressure image onto a model surface in object space using the collinearity equations. Current PSP software maps pressure data onto a CAD grid of a model under an assumption that the model does not deformed in wind tunnel tests. Actually, the model undergoes considerable deformation due to aerodynamic loads. Thus, the pressure mapping on the presumed rigid body results in inaccurate representation of the pressure field and introduces a bias error. To solve this problem, Bell and Burner (1998) discussed the feasibility of integrating PSP with a videogrammetric model deformation (VMD) system and Liu et al. (1999a) further addressed some technical details of integration of these systems. It is technically feasible for PSP to integrate with VMD that provides a deformed surface grid for PSP mapping. In addition, the integration of PSP and VMD will enhance productivity and reduce cost for tests in large-scale production wind tunnels.

6. Uncertainty Analysis

Uncertainty estimates for PSP is highly desirable. The sensitivity analysis for PSP was given by Sajben (1993) and Oglesby *et al.* (1995a). Mendoza (1997) investigated CCD camera noise and its effect on PSP measurements. Studying radiative energy transport in PSP and modeling a CCD camera, Liu et al. (1999b) gave a more complete uncertainty analysis for PSP. Relevant uncertainty issues of PSP were also addressed in other literature (Morris *et al.* 1993, Crites 1993, Bukov *et al.* 1993, Liu *et al.* 1997a,

Mosharov et al. 1997). Cattafesta *et al.* (1998) gave, in parallel, uncertainty estimates for temperature sensitive paint (TSP) measurements with CCD cameras.

6.1. System modeling

A systematic study of PSP uncertainty needs a functional relation between the imaging system's output and other system parameters such as the camera performance parameters and PSP properties. Liu et al. (1999b) derived an expression for the number of photoelectrons generated in a photodetector by luminescence

$$n_{pe} = C \underbrace{\frac{\delta}{4} \frac{A_D t_{INT}}{F^2 (1+M_{op})^2}}_{\text{Optics}} \underbrace{c h \varphi(P,T)}_{\text{Pain}} \underbrace{I_0 \; K_1(\Delta\lambda_1)}_{\text{Excitation}} \underbrace{K_2(\Delta\lambda_2)}_{\text{Emission}}, \tag{11}$$

where n_{pe} is the number of the photoelectrons, A_D is the effective sensitive detector area, F is the f-number, M_{op} is the optical magnification, t_{INT} is the integration time, c is the luminescent molecule concentration, h is the paint thickness, $\varphi(P,T) = [k_1(T) + k_2(T)P]^{-1}$ is the luminescent quantum efficiency that only depends on pressure and temperature, I_0 is the intensity of excitation light, and C is a dimensional constant. The terms $K_1(\Delta\lambda_1)$ and $K_2(\Delta\lambda_2)$ are two integrals

$$K_1(\Delta\lambda_1) = \int_{\Delta\lambda_1} E_{\lambda_1}(\lambda_1)\left[1+\sigma_{rs}(\lambda_1)\right]d\lambda_1,$$

$$K_2(\Delta\lambda_2) = \int_{\Delta\lambda_2} \eta_{op}\,\eta_{atm}\,\alpha_{\lambda_2} E_{\lambda_2}(\lambda_2) R_g(\lambda_2) d\lambda_2,$$

where $E_{\ddot{e}_1}(\ddot{e}_1)$ and $E_{\ddot{e}_2}(\ddot{e}_2)$ are the shape functions of the spectra of the excitation light and luminescent emission, respectively, $\acute{o}_{rs}$ is a coefficient related to reflection and scattering of the excitation light on the wall, $\hat{o}_{op}$ and $\hat{o}_{atm}$ are the system's optical transmittance and atmospheric transmettance, respectively, $\hat{a}_{\ddot{e}_2}$ is the extinction coefficient of the PSP medium for the luminescent light, $R_q(\ddot{e}_2)$ is the detector's quantum efficiency, and $\ddot{A}\ddot{e}_2$ and $\ddot{A}\ddot{e}_1$ is the bandwidths of the filters used for the excitation light and luminescence, respectively. Physically, the terms $K_1(\ddot{A}\ddot{e}_1)$ and $K_2(\ddot{A}\ddot{e}_2)$ represent effects of optical filters on the excitation light and luminescent emission, respectively.

The system's voltage output V is $V = Gn_{pe}$, where G is the system's gain. Thus, an expression for detector voltage output is

$$V = \text{Đ}_c \text{Đ}_f \, hc I_0 [k_1(T) + k_2(T)P]^{-1}, \tag{12}$$

where

$$\text{Đ}_c = C \frac{\eth}{4} \frac{A_D t_{INT} G}{F^2 (1 + M_{op})^2} \text{ and } \text{Đ}_f = K_1(\ddot{A}\ddot{e}_1) K_2(\ddot{A}\ddot{e}_2).$$

The parameters Đ_c and Đ_f represent overall effects of the detector (e.g. camera) performance and filter parameters, respectively. When a ratio between a wind-on and wind-off (reference) images is taken, air pressure P can be expressed in terms of the system's output and other variables

$$P = U_1 \frac{V_{ref}(t, \boldsymbol{x})}{V(t', \boldsymbol{x}')} \frac{k_1(T_{ref}) + k_2(T_{ref}) P_{ref}}{k_2(T)} - \frac{k_1(T)}{k_2(T)}, \tag{13}$$

where

$$U_I = \frac{Đ_c}{Đ_{c\,ref}} \frac{Đ_f}{Đ_{f\,ref}} \frac{h(x')}{h_{ref}(x)} \frac{c(x')}{c_{ref}(x)} \frac{I_0(t', X')}{I_{0\,ref}(t, X)},$$

where $x = (x, y)^T$ and $x' = (x', y')^T$ are the coordinates in the wind-off and wind-on images, respectively, $X = (X, Y, Z)^T$ and $X' = (X', Y', Z')^T$ are the object space coordinates in the wind-off and wind-on cases, respectively, and t and t' are the instants at which the wind-off and wind-on images are taken, respectively. Here, the coordinates $x = (x, y)^T$ and $X = (X, Y, Z)^T$ are related through the collinearity equations. Unlike the generic Stern-Volmer equation used in previous PSP uncertainty estimates, the relation (13) describes a general case including model deformation, spectral variability, and temporal variations in both illumination and luminescence. This relation provides a framework for uncertainty analysis and allows a clear understanding of how these variables contribute the total uncertainty of PSP measurement.

In order to separate complicated coupling between the temporal and spatial variations of the variables, the relation (13) is simplified by considering a small model deformation and a short time interval. The wind-on image coordinates should generally be expressed as a superposition of the wind-off coordinates and displacement vector, i.e., $x' = x + Äx$. Similarly, the time decomposition is $t' = t + Ät$. For small $Äx$ and $Ät$, the ratio of CCD camera output voltage can be separated into two factors, that is, $V_{ref}(t, x)/V(t', x') \approx D_t(Ät)\, D_x(Äx)\, V_{ref}(t, x)/V(t, x)$, where the factor $D_t(Ät) = 1 - (\partial V/\partial t)(Ät)/V$ and $D_x(Äx) = 1 - (\nabla V) \cdot (Äx)/V$ represent effects of the temporal and spatial changes of the luminescent intensity, respectively. The temporal

change of the luminescent intensity may be caused by photodegradation and sedimentation of dusts and oil droplets on a surface. The spatial intensity change is due to model deformation. In the same fashion, the excitation light intensity is decomposed into $I_0(t',X')/I_{0ref}(t,X) \approx D_{I0}(\Ät)I_0(t,X')/I_{0ref}(t,X)$, where the factor $D_{I0}(\Ät) = 1 + (\partial I_0/\partial t)(\Ät)/I_{0ref}$ reflects the temporal variation in the excitation light intensity. The use of the above estimates yields the modified Stern-Volmer relation

$$\frac{P}{P_{ref}} = U_2 \frac{V_{ref}(t,\boldsymbol{x})}{V(t,\boldsymbol{x})} \frac{1}{B(T)} - \frac{A(T)}{B(T)}. \tag{14}$$

where

$$U_2 = D_t(\Ät)D_x(\Ä\boldsymbol{x})D_{I0}(\Ät)\frac{Đ_c}{Đ_{c\,ref}}\frac{Đ_f}{Đ_{f\,ref}}\frac{h(\boldsymbol{x}')}{h_{ref}(\boldsymbol{x})}\frac{c(\boldsymbol{x}')}{c_{ref}(\boldsymbol{x})}\frac{I_0(t,\boldsymbol{X}')}{I_{0ref}(t,\boldsymbol{X})}.$$

In an ideal case where the wind-on and wind-off images are completely matched ($\boldsymbol{x}' = \boldsymbol{x}$), the factor U_2 is unity and Eq. (14) recovers the generic Stern-Volmer relation.

6.2. Error propagation and sensitivity

According to general uncertainty analysis formalism (Ronen 1988, Bevington and Robinson 1992), the relative variance of pressure P is described by the error propagation equation

$$\frac{var(P)}{P^2} = \sum_{i,j=1}^{M} S_i S_j \tilde{n}_{ij} \frac{[var(æ_i)var(æ_j)]^{1/2}}{æ_i æ_j}, \tag{15}$$

where $\tilde{n}_{ij} = cov(æ_i æ_j)/[var(æ_i)var(æ_j)]^{1/2}$ is the correlation coefficient between the variables $æ_i$ and $æ_j$, $var(æ_i) = <\Äæ_i^2>$ and $cov(æ_i æ_j) = <\Äæ_i \Äæ_j>$ are the variance and covariance, respectively, and the notation $<>$ denotes the statistical assemble

average. The variables $\{\alpha_i, i = 1 \cdots M\}$ denotes a set of the parameters $D_t(\Delta t)$, $D_x(\Delta x)$, $D_{I0}(\Delta t)$, V, V_{ref}, $\Phi_c/\Phi_{c\,ref}$, $\Phi_f/\Phi_{f\,ref}$, h/h_{ref}, c/c_{ref}, $I_0/I_{0\,ref}$, P_{ref}, T, A and B. The sensitivity coefficients S_i, defined as $S_i = (\alpha_i/P)(\partial P/\partial \alpha_i)$, are listed in Table I along with the corresponding elemental errors and the physical origins of the errors. Many sensitivity coefficients are proportional to a factor $1 + [A(T)/B(T)]/(P/P_{ref})$. For simplicity, the cross-correlation coefficients $\rho_{i\,j}\ (i \neq j)$ are usually assumed to be zero.

The elemental uncertainties in these variables have different physical origins. The uncertainties in V and V_{ref} result from photodetector (e. g. camera) noise. The uncertainties in $\Phi_c/\Phi_{c\,ref}$ and $\Phi_f/\Phi_{f\,ref}$ are associated with the variations of the detector (e. g. camera) performance parameters and the spectral variability of an illumination source, respectively. The uncertainties in $D_x(\Delta x)$, h/h_{ref}, c/c_{ref}, and $I_0/I_{0\,ref}$, are caused by model deformation. The errors in $D_t(\Delta t)$ and $D_{I0}(\Delta t)$ are attributed to the temporal variations in the luminescent emission and excitation light, respectively. The uncertainties in A and B represent PSP calibration errors in determination of these coefficients in either *a priori* pressure chamber tests or in-situ wind tunnel tests. Temperature effect is always a significant error source. Many of these errors are bias errors and others like the photon shot noise are random errors. The error propagation equation (15) does not include the uncertainty in pressure mapping. It must be taken into account in a final estimate of the total PSP uncertainty.

6.3. Elemental error sources

Photodetector noise and limiting pressure resolution

The uncertainties in V and V_{ref} are contributed from various noise sources in a photodetector (camera) such as photon shot noise, dark current shot noise, amplifier noise, quantization noise, and pattern noise (Holst 1996). For system analysis, the amplifier noise and other noises are conveniently treated as a single quantity — the noise floor. In principle, the noise floor and pattern noise can be reduced such that the detector (CCD camera) system is photon-shot-noise-limited. Thus, the photon-shot-noise-limited SNR is $SNR = \sqrt{n_{pe}}$. The uncertainties in the output voltages are $var(V) = 1/n_{pe}$ and $var(V_{ref}) = 1/n_{peref}$. In a limiting case where the uncertainty of pressure is solely dominated by the photon shot noise, the error propagation equation (15) contains only two terms related to V and V_{ref}. When a photodetector achieves the maximum capability such as the full-well capacity for a CCD camera, one obtains the minimum pressure difference that the camera can measure from a single frame of image

$$\frac{(\ddot{A}P)_{min}}{P} = \frac{1}{\sqrt{(n_{peref})_{max}}}\left[1 + \frac{A(T)}{B(T)}\frac{P_{ref}}{P}\right]\left[1 + A(T) + B(T)\frac{P}{P_{ref}}\right]^{1/2}, \qquad (16)$$

where $(n_{peref})_{max}$ is the maximum number of photoelectrons achieved by a photodetector in the reference condition such as the full-well capacity for a CCD camera. For scientific-grade CCD cameras, the full-well capacity varies from 250,000 to 700,000 electrons, while a standard video CCD camera typically has the full well capacity of 40,000 electrons. The formula (16) provides an estimate for the noise-equivalent pressure resolution for a photodetector including CCD camera. The minimum uncertainty in the non-dimensional pressure coefficient can be accordingly obtained from Eq. (16) as a

function of Mach number. Since the photon shot noise is a random noise, the limiting pressure difference can be further reduced by a factor $N^{1/2}$ when N images are averaged.

Errors induced by model deformation

Model deformation due to aerodynamic loads causes serious problems for the image ratio method since the wind-off and wind-on images are not spatially matched. Consider the displacement vector $\ddot{A}\boldsymbol{x} = \boldsymbol{x}' - \boldsymbol{x}$ between the wind-on and wind-off image coordinates. This displacement leads to a deviation of $D_x(\ddot{A}\boldsymbol{x})$, h/h_{ref}, c/c_{ref}, and I_0/I_{0ref} from unity. The uncertainties in $D_x(\ddot{A}\boldsymbol{x})$, h/h_{ref}, and c/c_{ref} are related to the distributions of the luminescent intensity, paint thickness, and dye concentration on a surface. Without the image registration, the uncertainties are unacceptably large for quantitative measurements. After the image registration is applied, the estimated variances of $D_x(\ddot{A}\boldsymbol{x})$, h/h_{ref}, and c/c_{ref} are $var[D_x(\ddot{A}\boldsymbol{x})] \approx W(V)/V^2$, $var(h/h_{ref}) \approx W(h)/(h_{ref})^2$, and $var(c/c_{ref}) \approx W(c)/(c_{ref})^2$. The operator $W(\bullet)$ is defined as $W(\bullet) = (\partial/\partial x)^2 \acute{o}_x^2 + (\partial/\partial y)^2 \acute{o}_y^2$, where $\acute{o}_x$ and $\acute{o}_y$ are the standard deviations of least-squares estimation in the image registration.

The uncertainty in $I_0(\boldsymbol{X})/I_{0ref}(\boldsymbol{X}')$ is caused by a change in illumination intensity on a model surface after the model moves with respect to light sources. This error cannot be corrected by the image registration since illumination light field is only a function of the object space coordinates. When a point on the model surface travels in the displacement vector $\ddot{A}\boldsymbol{X} = \boldsymbol{X}' - \boldsymbol{X}$ in object space, the variation in illumination intensity at this point is $\ddot{A}[I_0(\boldsymbol{X})/I_{0ref}(\boldsymbol{X}')] \approx (\nabla I_0)\bullet(\ddot{A}\boldsymbol{X})/I_{0ref}$, where $\boldsymbol{X} = (X, Y, Z)^T$ and $\boldsymbol{X}' = (X', Y', Z')^T$

are the coordinates of this point in object space in the wind-off and wind-on cases, respectively. Thus, the variance of I_0/I_{0ref} is

$$var[I_0(X)/I_{0ref}(X')] \approx (I_{0ref})^{-2}|(\nabla I_0)\bullet(\Delta X)|^2.$$

Consider a point light source with an intensity distribution $I_0(X - X_s) = |X - X_s|^{-n}$, where n is an exponent and $|X - X_s|$ is the distance between the point X on a model surface and the light source location X_s. The variance of I_0/I_{0ref} for a single point source is

$$var[I_0(X)/I_{0ref}(X')] = n^2|X - X_s|^{-4}|(X - X_s)\bullet(\Delta X)|^2.$$

The variance for multiple point light sources can be obtained based on the principle of superposition. In addition, model deformation may modify the camera performance parameters since the distance between the model surface and the camera lens is slightly changed. This change leads to the uncertainty of $var(\Delta_c/\Delta_{cref}) \approx [R_2/(R_1 + R_2)]^2(\Delta R_1/R_1)^2$, where R_1 is the distance between the lens and model surface and R_2 is the distance between the lens and CCD. When $R_1 >> R_2$, this error is very small.

Temperature effects

Since PSP is intrinsically temperature-dependent, surface temperature change during wind tunnel runs results in considerable uncertainty in PSP measurement. In order to correct the temperature effect of PSP, temperature-sensitive paint (TSP) is used to provide a distribution of surface temperature. For typical TSPs, the uncertainty in temperature measurement is between 0.2 and 0.8 °C (Liu *et al.* 1997a). Furthermore,

temperature changes the total uncertainty of PSP measurement by altering the sensitivity coefficients of the variables in the error propagation equation (15). The temperature hysteresis may occur for certain polymers and it may affect PSP measurement (Liu *et al.* 1995).

Calibration errors

The uncertainties in the Stern-Volmer coefficients A and B are calibration errors. In *a priori* PSP calibration in a pressure chamber, the uncertainty is represented by the standard deviation of data collected in replication tests. Because the tests in a pressure chamber are well controlled, *a priori* calibration result shows small precision error. However, significant bias error is usually found in wind tunnel tests when the *a priori* laboratory calibration result is used for data reduction. In contrast, *in-situ* calibration utilizes data from pressure taps distributed over a model surface in wind-tunnel runs to determine the Stern-Volmer coefficients. The *in-situ* calibration considerably reduces some bias errors and naturally achieves good fit to pressure tap data. On the other hand, since the model is not isothermal, the spatial variation in surface temperature may complicate the *in-situ* calibration and produce the position-dependent calibration results. Generally, the uncertainty in paint calibration is characterized by the standard deviation in fitting calibration data.

Temporal variations in luminescence and illumination

For PSP measurements in steady flows, the temporal change in luminescent intensity mainly results from photodegradation and sedimentation of dusts and oil droplets on a model surface. Photodegradation of PSP may occur when there is a considerable exposure to the excitation light between the wind-off and wind-on measurements. Dusts

and oil droplets in air sediment on a model surface during wind-tunnel runs. The resulting dust/oil layer absorbs both the excitation light and luminescent emission and changes light scattering on the surface. Despite the very different physical origins, both photodegradation and dust/oil contamination cause a decrease of luminescent intensity with time. Hence, the uncertainty in $D_t(\ddot{A}t)$ due to these effects can be collectively characterized by the variance $var[D_t(\ddot{A}t)] \approx [(\partial V/\partial t)(\ddot{A}t)/V]^2$. Similarly, the uncertainty in $D_{I0}(\ddot{A}t)$ produced by an unstable excitation light source is described by $var[D_{I0}(\ddot{A}t)] \approx [(\partial I_0/\partial t)(\ddot{A}t)/I_{0ref}]^2$.

Spectral variability and filter leaking

The uncertainty in $\eth_f/\eth_{f\,ref}$ is mainly attributed to spectral variability in the illumination light and spectral leaking of the filters. Possolo and Maier (1998) observed the spectral variability between flashes of a xenon lamp and studied its effect on PSP measurements. They found that the uncertainties in the absolute pressure and pressure coefficient due to the flash spectral variability is 0.05 psi and 0.01, respectively. A larger number of simultaneously flashing lamps lead to smaller effect of their spectral variability. This is another form of assemble averaging to reduce measurement uncertainties. Therefore, it is suggested to use multiple flash lamps for illumination. Optical filters are used to separate luminescence from excitation light. If the filters are not selected appropriately, a small portion of photons from the excitation light and ambient light may reach the detector through the filters and produce an additional voltage output.

Pressure mapping errors

The uncertainties in pressure mapping are related to the last data reduction procedure in which PSP data in 2D image are mapped onto a model surface in 3D object space. They include errors in camera calibration and mapping on the surface of a presumed rigid body. Although these errors are not included in the error propagation equation (15), they must be taken into account in the total uncertainty estimate. The camera calibration error is represented by the standard deviation of the calculated target coordinates in image plane. Typically, the optimization method gives the standard deviation of 0.04 pixels in image plane compared to 2.5 pixels given by the standard DLT for a lens with moderate radial lens distortion. For a given pressure image, the pressure variance induced by the camera calibration error is estimated by $var(P) \approx (\partial P/\partial x)^2 \acute{o}_x^2 + (\partial P/\partial y)^2 \acute{o}_y^2$, where $\acute{o}_x$ and $\acute{o}_y$ are the standard deviations of the calculated target coordinates in image plane.

Current PSP systems map pressure data onto a surface of a non-deformed model. However, in wind tunnel tests, a model undergoes considerable deformation due to aerodynamic loads (Burner 1997, Liu *et al.* 1999a). Obviously, PSP mapping on a non-deformed surface grid leads to another deformation-related error. If the displacement vector of a point on the model surface in object space is $\ddot{A}\boldsymbol{X} = \boldsymbol{X}' - \boldsymbol{X}$, the pressure variance induced by mapping on a rigid body without considering deformation is $var(P) = \left|(\nabla P)_{surf} \bullet (\ddot{A}\boldsymbol{X})_{surf}\right|^2$, where $(\nabla P)_{surf}$ is the pressure gradient on the surface and $(\ddot{A}\boldsymbol{X})_{surf}$ is the projected component of the displacement vector on the surface. In order to eliminate this error, we have to measure model deformation and generate a deformed

surface grid for correct PSP mapping. Bell and Burner (1998) and Liu *et al.* (1999a) have discussed integration of a PSP system with a model deformation measurement system.

Other error sources

Other error sources include self-illumination, paint intrusiveness, limiting time response, and induction effect. Self-illumination is a phenomena that luminescence from one part of a model surface reflects to another surface, thus distorting the observed luminescent intensity by superposing all the rays reflected from other points. It often occurs on surfaces of neighbor components of a complex model. Ruyten (1997) discussed this problem and gave a numerical correction procedure for self-illumination. Paint layer with a non-homogenous thickness modifies the shape of a model such that the surface pressure distribution may be slightly changed. Hence, this paint intrusiveness should be considered as an error source in PSP measurement. In PSP applications in unsteady flows, the limiting time response imposes an additional restriction on accuracy of PSP. The time response of PSP is mainly determined by oxygen diffusion process through PSP. The time response of some PSPs to pressure changes were studied by Baron et al. (1993), Engler (1995), Carroll et al. (1995, 1996), and Winslow et al. (1996). Another problem related to the time response is the 'induction effect' defined as an increase in luminescence during the first few minutes of illumination. This effect has been observed with certain paints and the photochemical process behind it has been explained by Uibel et al. (1993) and Gouterman (1997).

7. PSP Applications

7.1. Subsonic, transonic, and supersonic flows

Most PSP measurements on aerodynamic models have been conducted in subsonic, transonic and supersonic flows since PSP, in principle, is more effective in a range of Mach number from 0.3 to 3.0. Kavandi et al. (1990) and McLachlan et al. (1993) tested a NACA-0012 airfoil over a Mach number range of 0.3 to 0.66 at NASA Langley. A shock on the model upper surface was clearly identified at Mach 0.66. Comparison of the PSP results to conventional pressure tap measurement was good when *in-situ* calibration was applied. McLachlan et al. (1995a, 1995b) also tested a large generic transport wing/body configuration at Mach numbers between 0.7 to 0.9 and a high-sweep oblique wing model at Mach numbers between 1.6 and 2.0. Their PSP data shows complex two-dimensional pressure distributions containing rich information that would be difficult to deduce from the discrete tap data. Complemented with other flow visualization techniques such as schlieren imaging, surface oil flow and water tunnel visualization, PSP provides a deep understanding of physical mechanisms behind these aerodynamic flows. Researchers at McDonnell Douglas have conducted PSP measurements on a generic wing/body model at Mach 2, a high performance fighter model at Mach 1.2, and a two-dimensional converging/diverging nozzle (Morris et al. 1993b, Dowgwillo et al. 1994). They also measured the pressure distributions in shock/turbulent boundary layer interaction (Donovan 1992, Morris et al. 1993b) and sonic-jet/free-stream interaction at Mach 1.6 (Everett et al. 1995). Sellers and Brill (1994) and Sellers (1998) measured the pressure distributions on an aircraft model using PSP in the Arnold Engineering Development Center transonic wind tunnel. Their PSP data achieved good agreement with conventional pressure measurements and CFD computations. The two-component PSP developed by TsAGI was used on a civil aircraft model at Mach 0.8 in

ONERA (Lyonnet et al. 1997). The PSP data were carefully compared with conventional pressure tap results and the accuracy of PSP measurements was evaluated. This study clearly shows the feasibility of routine use of the two-component PSP in a large-scale production wind tunnel. Considerable work conducted at TsAGI has been reviewed by Bukov et al. (1993), Troyanovsky et al. (1993), Bykov et al. (1997), and Mosharov et al. (1997). Experiments on PSP in British Aerospace, DERA, and DLR were described by Davies et al. (1995), Holmes (1998), and Engler et al. (1997), respectively. It is noted that Davies's work is mainly based on the use of a laser-scanning lifetime system and Holmes uses a fluorescent lifetime imaging system.

An effort to study the effects of boundary layer control in supersonic inlets using small blowing jets have been studied at NASA Lewis Research Center. These tests conducted in the Lewis 1 foot by 1 foot Supersonic Wind Tunnel (SWT) looked at the shock wave/boundary layer interactions that cause a reduction in the inlet performance due to boundary layer separation. The test setup consists of replacing a wind tunnel sidewall panel with the boundary layer control device. The amount of surface blowing was varied using a control valve on the facility high-pressure air system. These panels were painted with a silicone based Ruthenium PSP. Reference images were taken at reduced pressure since this facility has the capability to be brought to near vacuum conditions quickly. Wind-on data images were acquired at varying Mach numbers and blowing mass flow rates. Reduction of the acquired data was performed using the classical intensity based method and in-situ calibrated from pressure taps located in the painted sections. Figures 5 and 6 show PSP images for two surface blowing configurations. Figure 5 shows a recessed blowing configuration where the blowing air is

introduced from an aft facing step in the wall section while Figure 6 introduces the air from a protruding nozzle in the wall section. Significant spatial details are apparent that are not feasible with other types of pressure instrumentation.

7.2. Hypersonic flows

Hypersonic flows are difficult areas in PSP applications. High enthalpy in hypersonic flows may produce significant temperature increase on a model surface. Large absolute pressure in the pressure side of the model causes weak luminescent emission and thus leads to low SNR. High shear stress imposes additional constraints to the mechanical properties of PSP and a thin coating is required to sustain high skin friction. In particular, since hypersonic wind tunnels are usually short-duration tunnels, PSP must have a short response time. The short run-time limits the exposure time of a CCD camera to collect photons and further reduces SNR. Some PSP measurements were made in hypersonic flows and the results are still in preliminary nature. Using fast-responding PSPs developed at TsAGI, Troyanovsky et al. (1993) carried out a semi-quantitative pressure visualization for shock/body interaction in a Mach 8 shock tube with 0.1 s duration, and Borovoy et al. (1995) determined the pressure distributions on a cylinder at Mach 6 in a shock wind tunnel with about 40 ms duration. Borovoy's results are fairly consistent with calculation and pressure transducer measurements. Jules et al. (1995) used a McDonnell Douglas PSP to study shock/boundary-layer interaction over a flat-plate/conical-fin configuration at Mach 6. Their PSP data show a systematic shift compared to pressure tap measurements. Recently, Hubner et al. (1997, 1999) measured the pressure distributions on a wedge and an elliptic cone at Mach 7.5 in the Calspan hypersonic shock tunnel. The run-time of the tunnel for the PSP test is only 7-8 ms. In order to minimize the

temperature effect of PSP, they applied directly PSP on the metal model surface rather than a white base-coat. However, because of the lack of a white base-coat and the thin-layer application of PSP, luminescent intensity of PSP was relatively low and only 5 to 12% of the CCD full-well capacity was utilized. Buck (1994) reviewed hypersonic PSP and TSP work done at NASA Langely.

7.3. Low-speed flows

Low-speed flow (Mach number is less than 0.2) is a limiting case in PSP measurements since a change in air pressure is very small. The major error sources, notably temperature effect, image misalignment and CCD camera noise, must be minimized to obtain acceptable quantitative results. Using a laser-scanning system, Torgerson et al. (1996) assessed the feasibility of PSP measurement in a low-speed impinging jet. They utilized three different methods: intensity ratioing, phase sensitive detection, and dual-luminophore paint. They found that temperature effect, image misalignment, and non-uniformity attributed to polymer microhetrogeneity may significantly degrade the accuracy of PSP measurement in low-speed flows. Using a 14-bit CCD camera, Brown et al. (1997) conducted PSP measurements on a NACA 0012 airfoil in very low speeds (less than 50 m/s). They carefully reduced the movement of the measurement system relative to the model by firmly mounting the camera to the test section. The tunnel runs for a long time period before data acquisition in order to achieve a thermal equilibrium in free-stream. Also, the wind-off image was taken immediately after the wind-on image to minimize effect of temporal variation of free-stream temperature. Their experiments show that temperature and registration effects are significant error sources in low-speed flow PSP measurements. Careful experimental

procedures are needed to control these error sources. After all efforts made to reduce these errors, they obtained reasonably good pressure results at speeds as low as 20 m/s. On the other hand, however, their study shows how difficult it is to use PSP in low-speed flows in an industrial production wind tunnel where many factors affecting the accuracy of PSP measurement are uncontrollable. Bell et al. (1998) conducted low-speed PSP measurements in production wind tunnels at NASA Ames. They also concluded that the most significant errors are due to temperature sensitivity and model motion. Other researchers have used PSPs in several low-speed flows. Morris (1995) measured the pressure distributions on delta wings in low-speed flows. These results indicate the low-pressure regions induced by leading-edge vortices. Good agreement is shown between PSP measurements and tap measurements. Verhaagen et al. (1995) used PSP to study the vortex flow over a double delta wing. Dale et al. (1998) recently conducted preliminary PSP measurements on a turret model at speeds at as low as 12 m/s. Using a laser-scanning lifetime system, Davies et al. (1995) measured the surface pressure on a cylinder at 80 m/s.

7.4. Rotating machinery

PSP is a promising non-contact technique for measuring surface pressure distributions on high-speed rotating blades in rotating machinery where conventional instrumentation is particularly difficult. PSP measurements on rotating machinery were conducted by Burns and Sullivan (1995) with a laser scanning system. They obtained the pressure distributions on a small wooden propeller at a rotational speed of 3120 rpm and a TRW Hartzell propeller at a rotational speed of 2360 rpm. The PSP-derived pressure coefficient distributions across the blades show a reasonable trend. Using the laser-

scanning system, Liu et al. (1997b) and Torgerson et al. (1997) performed PSP measurements on rotor blades in a high-speed axial flow compressor and an Allied Signal F109 turbofan engine. PSP and TSP were applied to alternating blades, where TSP provides the temperature distributions on the blades for temperature correction of PSP. They obtained the pressure and temperature maps on the blade surfaces at different rotational speeds. The pressure distributions clearly indicate the formation of a shock on the surface as rotational speed is increased. Moshasrov et al. (1997) described PSP measurements on propellers and rotating machinery at TsAGI. Using a CCD camera system with a pulse light source, they obtained pressure distributions on propellers. PSP measurements on the helicopter rotor blades were carried out at TsAGI (Bykov et al. 1997, Moshasrov et al. 1997) and NASA Ames (Schairer et al. 1998). Hubner et al. (1996) suggested a lifetime imaging method for pressure measurements on rotating machinery. This method is based on detecting the luminescent decay traces of a rotating painted surface on a CCD camera.

Full field rotating pressure and temperature measurements were made on blades of a 24-inch diameter scale-model fan in the NASA Lewis Research Center 9-foot by 15-foot low speed wind tunnel at rotational speeds as high as 9500 RPM (Bencic 1997). The 25% scale model used for this work was a single rotation, ultra high bypass fan. The intent of this particular test article was to evaluate a reduced tip speed fan for its acoustic signature while keeping fan performance similar to higher speed fans. The experiment was carried out by painting two blades, one with TSP and the other with PSP. The fan was operated over its designed conditions and data taken at each condition of interest. The traditional intensity based method for PSP and TSP acquisition was used requiring two images for

each paint, a reference image and a data were used to determine the pressure and temperature profiles. The illumination of the PSP and TSP was performed by multiple filtered and focused xenon flashlamps. A two microseconds flash duration yielded approximately 0.5mm of blurring at the highest speeds. This amount was deemed acceptable for this test. Images were acquired using multiple flashes integrated over two hundred revolutions while the camera shutter was kept open to achieve an acceptable CCD well capacity. The painted fan blades installed in the fan test rig are shown in Figure 7. The TSP images were used to correct temperature effect on the PSP data. The temperature profiles at four speeds on the fan operating line are shown in Figure 8 and the corresponding temperature-corrected pressure images are shown in Figure 9.

7.5. Cryogenic wind tunnels

PSP has recently been demonstrated for use in cryogenic wind tunnels where oxygen concentration is extremely low and temperature is as low as 90 K (Asai et al. 1997, Upchurch et al. 1998). The development of cryogenic PSP is initiated by the need of PSP that can be used in large-scale pressurized cryogenic wind tunnels such as the National Transonic Facility (NTF) at NASA Langley and the European Transonic Wind Tunnel (ETW). Campbell et al. (1994) first found that some luminophores in very porous binders such as silica gel and alumina could be quenched at cryogenic temperatures. This finding leads to the invention of several cryogenic TSPs and successful applications of these paints for boundary-layer transition detection in cryogenic wind tunnels (Asai et al 1996). Asai et al (1997) first developed a matrix-free PSP coating on an anodized aluminum surface and measured the surface pressure distributions on a 14% thick circular-arc bump model in a cryogenic wind tunnel. PSP data at Mach numbers of 0.75-0.84 and

a temperature of 100 K are in good agreement with pressure tap data. However, the methodology of coating on an anodized surface is not applied to stainless steel of which models for cryogenic wind tunnel testing are usually made. Upchurch et al. (1998) developed a polymer-based cryogenic PSP that is universally applicable to all types of surfaces including stainless steel. This paint has been applied to a test in the 0.3m cryogenic tunnel at NASA Langley.

7.6. Flight tests

McLachlan et al. (1992) used a standard 8-bit video camera mounted in an F-104G aircraft flying between Mach 1.0 to 1.6 to measure the pressure distribution of a window coated with PSP. Houck et al. (1996) conducted a flight test to image the pressure distribution on a practice bomb coated with PSP. They used a film camera and the film was later processed and digitized for data reduction. Using a portable 2D laser-scanning system, Lachendro et al. (1998) conducted in-flight PSP measurements on a wing of a Beechjet 400A aircraft at Mach 0.75 and altitude of 31,000 ft. PSP and TSP trips were attached on the wing surface. The laser scanning system is optically modulated and is capable of both phase and intensity based measurements. The intensity-based measurements fail because of wing deformation in flight. Phase-based PSP measurements showed the same trend as flight test data provided by the National Aerospace Laboratory of Japan (NAL).

8. Conclusions

Pressure sensitive paint (PSP) is an innovative technique for global surface pressure measurement. The full-field mapping capability of PSP allows an understanding

of complicated phenomena in aerodynamic flows that cannot be easily induced by using conventional techniques. PSP has been used for surface pressure measurements on a variety of models over a wide range of Mach numbers in wind tunnels. Improvements have being made in all the technical areas of PSP including paint formulation, illumination, imaging, and data acquisition/processing hardware and software. Considerable effort has been recently made to develop low-temperature-sensitive PSP, multiple-luminophore PSP, and cryogenic PSP. The newly developed fluorescent lifetime imaging system is promising to avoid the deformation-induced problems in the image ratio method. The modeling and uncertainty analysis of a PSP system have been given that is useful for optimal design of PSP experiments in wind tunnels. New advances have been made in several more difficult areas of PSP applications such as low-speed flows, rotating machinery, cryogenic wind tunnels and flight tests. In the future, PSP system will be further integrated with videogrammetric model deformation system and other modern optical measurement techniques for aerodynamic testing.

Acknowledgment:

This work was supported by ONR, AFOSR, NASA Langley, NASA Ames, NASA Lewis and the Boeing Company. We would like to thank Nathan Lachendro of Purdue University for providing PSP calibration results.

References:

Abdel-Aziz, Y. I. and Karara, H. M. (1971), Direct linear transformation from comparator coordinates into object space coordinates in close-range photogrammetry, Proc. ASP/UI Symp. on Close-Range Photogrammetry, Univ. of Illinois at Urbana-Champaign, Urbana, Illinois, 1-18.

Ardasheva, M. M., Nevskii, L. B. and Pervushin, G. E. (1985), Measurement of Pressure Distribution by Means of Indicator Coatings, Journal of Applied Mechanics and Technical Physics, No. 4, 24-33.

Asai, K., Kanda, H., Kunimasu, T., Liu, T. and Sullivan, J. (1996), Detection of Boundary-Layer Transition in a Cryogenic Wind Tunnel by Using Luminescent Paint, AIAA Paper 96-2185.

Asai, K., Kanda, H., Cunningham, C. T., Erausquin, R., and Sullivan, J. (1997), Surface pressure measurement in a cryogenic wind tunnel by using luminescent coating, ICIASF '97 Record, International Congress on Instrumentation in Aerospace Simulation Facilities, Pacific Grove, CA, September 29-October 2, 105-114.

Baron, A. E., Danielson, J. D., Gouterman, M., Wan, J., Callis, J. B. and McLachlan, B. (1993), Submillisecond Response Times of Oxygen-Quenching Luminescent Coatings, Rev. Sci. Instrum. 64(12), 3394-3402.

Bell, J. H. and McLachlan, B. G. (1993), Image Registration for Luminescent Paint Sensors, AIAA Paper 93-0178.

Bell, J. H. and Burner, A. W. (1998), Data fusion in wind tunnel testing: Combined pressure paint and model deformation measurements, AIAA Paper 98-2500.

Bell, J., Schairer, E., Mehta, R., and Hand, L. (1998), Low speed PSP testing in production wind tunnels, Proceeding of the Sixth Annual Pressure Sensitive Paint Workshop, The Boeing Company, Seattle, Washington, October 6-8, 17-1 to 17-17.

Bennett, R. G. and McCartin, P. J. (1966), Radiationless Deactivation of the Fluorescent State of Substituted Anthracences, The Journal of Chemical Physics, Vol. 44, No. 5, 1969-1973.

Bencic, T. (1997), Rotating pressure measurements on a scale model high-by-pass ratio fan using PSP at NASA LeRC, Proceeding of the Sixth Annual Pressure Sensitive Paint Workshop, Arnold Engineering Development Center, Tullahoma, Tennessee, May 14-16.

Bevington, P. R. and Robinson, D. K. (1992), Data reduction and error analysis for the physical sciences (Second edition), McGraw-Hill, Inc., New York.

Borovoy, V., Bykov, A., Mosharov, V., Orlov, A., Radchenko, V. and Phonov, S. (1995), Pressure Sensitive Paint Application in Shock Wind Tunnel, ICIASF '95 Record, International Congress on Instrumentation in Aerospace Simulation Facilities, Wright-Patterson Air Force Base, Dayton, OH, USA, 34.1-34.4.

Brown, O. C., Mehta, R. D., and Cantwell, B. J. (1997), Low-speed flow studies using the pressure sensitive paint technique, AGARD Conference Proceedings CP-601: Advanced Aerodynamic Measurement Technology, 31-1 to 31-13.

Buck, G. M. (1994), Simultaneous Luminescence Pressure and Temperature Measurements on Dyed Ceramic Models for Hypersonic Wind Tunnels, AIAA Paper 94-2482.

Bukov, A. P., Orlov, A. A., Mosharov, V. E., Radchenko, V. N. and Pesetsky, V. A. (1992), Application of Luminescence Quenching for Pressure Field Measurements on the Model Surface in Wind Tunnel, Proc. Wind Tunnels and Wind Tunnel Test Techniques Conf., Royal Aeronautical Society, London, U. K., pp. 8.1-8.11.

Bukov, A., Mosharov, V., Orlov, A., Pesetsky, V., Radchenko, V., Phonov, S., Matyash, S., Kuzmin, M. and Sadovsky, N. (1993), Optical Surface Pressure Measurements: Accuracy and Application Field Evaluation, 73th AGARD Fluid Dynamics Panel Meeting and Symposium on Wall Interference, Support Interference and Flow Field Measurements, Brussels, Belgium.

Burner, A. W., Radeztsky, R. H. and Liu, T. (1997), Videometric applications in wind tunnels," Videometrics V, Proceedings of The International Society for Optical Engineering (SPIE), Vol. 3174, San Diego, California, 234-247.

Burns, S. and Sullivan, J. (1995), The Use of Pressure Sensitive Paints on Rotating Machinery, ICIASF '95 Record, International Congress on Instrumentation in Aerospace Simulation Facilities, Wright-Patterson Air Force Base, Dayton, OH, USA, 32.1-32.14.

Bykov, A., Fonov, S., Mosharov, V., Orlov, A., Pesetsky, V., and Radchenko, V. (1997), Study result for the application of two-component PSP technology to aerodynamic experiment, AGARD Conference Proceedings CP-601, Advanced Aerodynamic Measurement Technology, 29-1 to 29-8.

Campbell, B., Liu, T. and Sullivan, J. (1994), Temperature Sensitive Fluorescent Paint Systems, AIAA Paper 94-2483.

Carroll, B. F., Winslow, A., Abbitt, J., Schanze, K. and Morris, M. (1995), Pressure Sensitive Paint: Application to a Sinusoidal Pressure Fluctuation, ICIASF '95 Record, International Congress on Instrumentation in Aerospace Simulation Facilities, Wright-Patterson Air Force Base, Dayton, OH, USA, 35.1-35.6.

Carroll, B. F., Abbitt, J. D., Lukas, E. W. and Morris, M. J. (1996), Step Response of Pressure Sensitive Paints, AIAA J, Vol. 34, No. 3, 521-526.

Cattafesta, L., Liu, T., and Sullivan, J. (1998), Uncertainty estimates for temperature sensitive paint measurements with CCD cameras, *AIAA J.* Vol. 36, No. 11, 2102-2108.

Clinehens, G. A. and Dale, G. A. (1998), Ultrastable blue-LED illumination sources for PSP applications, Proceeding of the Sixth Annual Pressure Sensitive Paint Workshop, The Boeing Company, Seattle, Washington, October 6-8, 22-1 to 11-9.

Crites, B. C. (1993), Measurement Techniques ---- Pressure Sensitive Paint Technique, Lecture Series 1993-05, von Karman Institute for Fluid Dynamics.

Dale G., Baust, H., Tyler, C., Jordan, J., Weaver, W., and Clinehens, G. (1998), Pressure sensitive paint measurements in very low-speed flows, Proceeding of the Sixth Annual Pressure Sensitive Paint Workshop, The Boeing Company, Seattle, Washington, October 6-8, 16-1 to 16-6.

Davies, A. G., Bedwell, D., Dunleavy, M. and Brownjohn, N. (1995), Pressure Sensitive Paint Measurements Using a Phosphorescence Lifetime Method, presented at Seventh International Symposium on Flow Visualization, September 11-14, Seattle, Washington.

Donovan, J. F. (1992), Preliminary Results From a Trangentially Injected Shock Wave/Turbulent Boundary Layer Interaction, presented at 13th Symposium on Turbulence, Rolla, MO.

Donovan, J. F., Morris, M. J., Pal, A., Benne, M. E. and Crites, R. C. (1993), Data Analysis Techniques for Pressure- and Temperature-Sensitive Paint, AIAA Paper 93-0176.

Dowgwillo, R. M., Morris, M. J., Donovan, J. F. and Benne, M. E. (1994), The Application of The Pressure Sensitive Paint Technique to High Speed Wind Tunnel Testing of a Fighter Aircraft Configuration With Complex Store Loadings, AIAA Paper 94-1932.

Engler, R. H. (1995), Further Developments of Pressure Sensitive Paint (OPMS) for Non Flat Models in Steady Transonic Flow and Unsteady Conditions, ICIASF '95 Record, International Congress on Instrumentation in Aerospace Simulation Facilities, Wright-Patterson Air Force Base, Dayton, OH, USA, 33.1-33.8.

Engler, R. H. and Klein, C. (1997), DLR PSP system: Intensity and lifetime measurements, ICIASF '97 Record, International Congress on Instrumentation in Aerospace Simulation Facilities, Pacific Grove, CA, September 29-October 2, 46-56.

Everett, D. E., Dutton, J. C. and Morris, M. J. (1995), Pressure Sensitive Paint Measurements of the Pressure Field about a Sonic Jet Injected Transversely into a Mach 1.6 Free Stream, AIAA Paper 95-0524.

Fisher, C. W., Linne, M. A., Middleton, N. T., Fiechtner, G., and Gord, J. (1999), Phase sensitive imaging in flows, AIAA Paper 99-0771.

Fraser, C. S. (1989), Optimization of networks in non-topographic photogrammetry, Chapter 8, Non-Topographic Photogrammetry, 2nd Edition, (H.M. Karara, editor), American Society for Photogrammetry and Remote Sensing, Falls Church, Virginia, 95-106.

Fraser, C. S. (1992), Photogrammetric camera component calibration — A review of analytical techniques, Workshop on Calibration and Orientation of Cameras in Computer Vision (TU-1), XVII Congress, International Society of Photogrammetry & Remote Sensing, Washington, DC.

Fryer, J. G. (1989), Camera calibration in non-topographic photogrammetry, Chapter 5, Non-Topographic Photogrammetry, 2nd Edition, (H.M. Karara, editor), American Society for Photogrammetry and Remote Sensing, Falls Church, Virginia, 59-69.

Gewehr, P. M. and Delpy, D. T. (1993), Optical Oxygen Sensor Based on Phosphorescence Lifetime Quenching and Employing a Polymer Immobilised Metalloporphyrin Probe, Medical & Biological Engineering & Computing, January, 2-21.

Gouterman, M., Callis, J., Burns, D., Kavandi, J., Gallery, J., Khalil, G., Green, E., McLachlan, B. and Crowder, J. (1990), Luminescence Imaging for Aerodynamic Testing, Proc. of the ONR/NASA Workshop on Quantitative Flow Visualization (J. Sullivan and B. Holmes), Purdue University, IN, USA.

Gouterman, M. (1997), Oxygen quenching of luminescence of pressure-sensitive paint for wind tunnel research, Journal of Chemical Education, Vol. 74, No. 6, June, 1-7.

Hamner, M., Campbell, B., Liu, T. and Sullivan, J. (1994), A Scanning Laser System for Temperature and Pressure Sensitive Paint, AIAA Paper 94-0728.

Harris, J. and Gouterman, M. (1995), Referenced Pressure Sensitive Paint, Flow Visualization VII, Proceeding of the Seventh International Symposium on Flow Visualization, edited by J. Crowder, Seattle, Washington, p.802.

Harris, J. and Gouterman, M. (1998), Referenced pressure sensitive paint using blue emitting phosphors, Proceeding of the Sixth Annual Pressure Sensitive Paint Workshop, The Boeing Company, Seattle, Washington, October 6-8, 19-1 to 19-13.

Hartmann, P. and Ziegler, W. (1996), Lifetime imaging of luminescent oxygen sensors based on all-solid-state technology, Analytical Chemistry, 68, 4512-4514.

Holmes, J. W. (1998), Analysis of radiometric, lifetime and fluorescent lifetime imaging for pressure sensitive paint, The Aeronautical Journal of the Royal Aeronautical Society, April, 189-194.

Holst, G. C. (1996), CCD arrays, cameras, and displays, SPIE Optical Engineering Press and JCD Publishing, Winter Park, FL.

Houck, S. W., Hepp, R. G., Morris, M. J., and Benne, M. E. (1996), Pressure sensitive paint flight test, IEEE Aerospace Applications Conference, Aspen Co, 3-10 Feb, Vol. 4, 241-252.

Hubner, J. P., Abbitt, J. D. and Carroll, B. F. (1996), Pressure Measurements on Rotating Machinery Using Lifetime Imaging of Pressure Sensitive Paint, AIAA Paper 96-2934.

Hubner, J., Carroll, B., Schanze, K., and Ji, H. (1997), Techniques for using pressure-sensitive paint in shock tunnel facilities, ICIASF '97 Record, International Congress on Instrumentation in Aerospace Simulation Facilities, Pacific Grove, CA, September 29-October 2, 30-39.

Hubner, J., Carroll, B., Schanze, K., Ji, H., and Holden, M. (1999), Temperature- and pressure-sensitive measurements in short-duration hypersonic flow, AIAA Paper 99-0388.

Jordan, J. D., Watkins, A. N., Weaver, W. L., Dale, G. A., and Navarra, K. R., (1999), Sol-gel-based pressure-sensitive paint development, AIAA Paper 99-0566, Reno, NV.

Jules, K., Carbonaro, M., and Zemsch, S. (1995), Application of pressure sensitive paint in hypersonic flows, NASA TM 106824.

Kavandi, J., Callis, J. B., Gouterman, M. P., Khalil, G., Wright, D., Green, E., Burns, D. and McLachlan, B. (1990), Luminescent Barometry in Wind Tunnels, Rev. Sci. Instrum. 61(11), 3340-3347.

Lachendro, N., Crafton, J., Guille, M., Sullivan, J., Carney, T. and Stirm, B.. (1998), Flight tests of pressure sensitive/temperature sensitive paint laser scanning system, Proceeding of the Sixth Annual Pressure Sensitive Paint Workshop, The Boeing Company, Seattle, Washington, October 6-8, 23-1 to 23-31.

Le Sant, Y. and Merienne, M-C. (1995), An image resection method applied to mapping techniques, ICIASF '95 Record, International Congress on Instrumentation in Aerospace Simulation Facilities, Wright-Patterson Air Force Base, Dayton, Ohio, July 18-21, 46.1-46.8.

Le Sant, Y., Deleglise, B., and Mebarki, Y. (1997), An automatics image alignment method applied to pressure sensitive paint measurements, ICIASF '97 Record, International Congress on Instrumentation in Aerospace Simulation Facilities, Pacific Grove, CA, September 29-October 2, 57-65.

Liu, T., Campbell, B. and Sullivan, J. (1995), Accuracy of temperature-sensitive fluorescent paint for heat transfer measurements, AIAA Paper 95-2042.

Liu, T., Campbell, B., Bruns, S., and Sullivan, J. (1997a), Temperature- and Pressure-sensitive luminescent paints in aerodynamics, Applied Mechanics Reviews, Vol. 50, No. 4, 227-246.

Liu, T., Johnston, R., Torgerson, S., Fleeter, S. and Sullivan, J. (1997b), Rotor Blade Pressure Measurement in a High Speed Axial Compressor Using Pressure and Temperature Sensitive Paints, AIAA Paper 97-0162

Liu, T., Radeztsky, R., Garg, S., and Cattafesta, L. (1999a), A videogrammetric model deformation system and its integration with pressure paint, AIAA Paper 99-0568.

Liu, T., Guille, M. and Sullivan, J. (1999b), Uncertainty analysis of pressure sensitive paint measurement, AIAA Paper 99-3785.

Lyonnet, M., Deleglise, B., Grenat, G., Modane, O., Bykov, A., Mosharov, V., Orlov, A. and Fonov, S. (1997), The two-component PSP investigation on a civil aircraft model in S2MA wind tunnel, AGARD Conference Proceedings CP-601: Advanced Aerodynamic Measurement Technology, 30-1 to 30-8.

McGlone, J. C. (1989), Analytic data-reduction schemes in non-topographic photogrammetry, Chapter 4, Non-Topographic Photogrammetry, 2nd Edition, (H.M. Karara, editor), American Society for Photogrammetry and Remote Sensing, Falls Church, Virginia, 37-55.

McLachlan, B. G., Bell, J. H. et al. (1992), Flight testing of a luminescent surface pressure sensor, NASA TM 103970.

McLachlan, B. G., Kavandi, J. L., Callis, J. B., Gouterman, M., Green, E. and Khalil, G. (1993), Surface Pressure Field Mapping Using Luminescent Coatings, Experiments in Fluids 14, 33-41.

McLachlan, B. G. and Bell, J. H. (1995a), Pressure-Sensitive Paint in Aerodynamic Testing, Experimental Thermal and Fluid Science, 10, 470-485.

McLachlan, B. G., Bell, J. H., Park, H., Kennelly, R. A., Schreiner, J. A., Smith, S. C., Strong, J. M., Gallery, J. and Gouterman, M. (1995b), Pressure-Sensitive Paint Measurements on Supersonic High-Sweep Oblique Wing Model, Journal of Aircraft, Vol. 32, No. 2, March-April, 217-227.

McLean, D. (1998), Referenced pressure paint and the ratio of ratios, Proceeding of the Sixth Annual Pressure Sensitive Paint Workshop, The Boeing Company, Seattle, Washington, October 6-8, 11-1 to 11-35.

Mendoza, D. R. (1997), An analysis of CCD camera noise and its effect on pressure sensitive paint instrumentation system signal-to-noise ratio, ICIASF '97 Record, International Congress on Instrumentation in Aerospace Simulation Facilities, Pacific Grove, CA, September 29-October 2, 22-29.

Morris, M. J., Benne, M. E., Crites, R. C. and Donovan, J. F. (1993a), Aerodynamics Measurements Based on Photoluminescence, AIAA Paper 93-0175.

Morris, M. J., Donovan, J. F., Kegelman, J. T., Schwab, S. D., Levy, R. L. and Crites, R. C. (1993b), Aerodynamic Applications of Pressure Sensitive Paint, AIAA Journal, Vol. 31, No. 3, March, 419-425.

Morris, M. J. (1995), Use of Pressure-Sensitive Paints in Low-Speed Flows, ICIASF '95 Record, International Congress on Instrumentation in Aerospace Simulation Facilities, Wright-Patterson Air Force Base, Dayton, OH, USA, 31.1-31.10.

Mosharov, V. E., Radchenko, V. N. and Fonov, S. D. (1997), Luminescent Pressure Sensors in Aerodynamic Experiments, Central Aerohydrodynamic Institute (TsAGI), CWA International Corporation, Moscow.

Oglesby, D. M., Puram, C. K. and Upchurch, B. T. (1995a), Optimization of Measurements With Pressure Sensitive Paints, NASA TM 4695.

Oglesby, D. M., Leighty, B. D. and Upchurch, B. T. (1995b), Pressure Sensitive Paint With an Internal Reference Luminiphore, Proceedings of the 41st International Instrumentation Symposium, Instrument Society of America, Denver, CO, 381-395.

Oglesby, D. M., Upchurch, B. T., Leighty, B. D. and Simmons, K. A. (1996), Pressure Sensitive Paint With Internal Temperature Sensing Luminiphore, Proceedings of the 42nd International Instrumentation Symposium, Instrument Society of America, San Diego, CA.

Peterson, J. I. and Fitzgerald, R. V. (1980), New Technique of Surface Flow Visualization Based on Oxygen Quenching of Fluorescence, Rev. Sci. Instrum. 51(5), 670-671.

Ponomarev, S. and Gouterman, M. (1998), Fast responding pressure sensitive paints based on high concentration of hard particles in polymer, Proceeding of the Sixth Annual Pressure Sensitive Paint Workshop, The Boeing Company, Seattle, Washington, October 6-8, 31-1 to 31-22.

Possolo, A. and Maier, R. (1998), Gauging uncertainty in pressure measurement due to spectral variability of excitation illumination, Proceeding of the Sixth Annual

Pressure Sensitive Paint Workshop, The Boeing Company, Seattle, Washington, October 6-8, 15-1 to 15-12.

Puklin, E., Carlson, B., Gouin, S., Costin, C., Green, E., Ponomarev, S., Tanji, H. and Gouterman, M. (1998), Ideal pressure sensitive paint: PtTFPP in FIB polymer, Proceeding of the Sixth Annual Pressure Sensitive Paint Workshop, The Boeing Company, Seattle, Washington, October 6-8, 8-1 to 8-22.

Ronen, Y. (1988), Uncertainty Analysis, CRC Press, Inc., Boca Raton, Florid.

Ruyten, W. M. (1997), Correcting luminescent paint measurements for self-illumination, ICIASF '97 Record, International Congress on Instrumentation in Aerospace Simulation Facilities, Pacific Grove, CA, September 29-October 2, 3-9.

Sacksteder, L., Demas, J. N. and DeGraff, B. A. (1993), Design of Oxygen Sensors Based on Quenching of Luminescent Metal Complexes: Effect of Ligand Size on Heterogeneity, Analytical Chemistry, Vol. 65, No. 23, December 1, 3480-3483.

Sajben, M. (1993), Uncertainty Estimates for Pressure Sensitive Paint Measurements, AIAA J., Vol. 31, No. 11, 2105-2110.

Schairer, E., Hand, L., Bell, J., and Mehta, R. (1998), Application of pressure-sensitive paint to helicopter rotors, Proceeding of the Sixth Annual Pressure Sensitive Paint Workshop, The Boeing Company, Seattle, Washington, October 6-8, 4-1 to 4-15.

Schanze, K. S., Carroll, B. F., Korotkevitch, S., and Morris, M. (1997), Temperature dependence of pressure sensitive paints, AIAA J., Vol. 35, No. 2, February, 306-310.

Sellers, M. E. and Brill, J. A. (1994), Demonstration Test of Pressure Sensitive Paint in the AEDC 16-ft Transonic Wind Tunnel Using the TST Model, AIAA Paper 94-2481.

Sellers, M. E. (1998), Pressure sensitive paint development at Arnold Engineering Development Center (AEDC), Proceeding of the Sixth Annual Pressure Sensitive Paint Workshop, The Boeing Company, Seattle, Washington, October 6-8, 2-1 to 2-19.

Song, L. and Fayer, M. D. (1991), Temperature Dependent Intersystem Crossing and Triplet-Triplet Absorption of Rubrene in Solid Solution, Journal of Luminescence 50, 75-81

Szmacinski, H. and Lakowicz, J. R. (1995), Fluorescence Lifetime-Based Sensing and Imaging, Sensors and Actuators B, 29, 16-24.

Torgerson, S. D., Liu, T. and Sullivan, J. P. (1996), Use of Pressure Sensitive Paints in Low Speed Flows, AIAA Paper 96-2184.

Torgerson, S. D., Liu, T., and Sullivan, J. P. (1997), Rotor blade pressure measurement in a rotating machinery using pressure and temperature sensitive paints, AGARD-CP-598, Advanced Non-Intrusive Instrumentation for Propulsion Engines, Brussels, Belgium, 20-24 October, 19-11 to 19-9.

Troyanovsky, I., Sadovskii, N., Kuzmin, M., Mosharov, V., Orlov, A., Radchenko, V. and Phonov, S. (1993), Set of Luminescence Pressure Sensors for Aerospace Research, Sensors and Actuators B, 11, 201-206.

Uibel, R., Khalil, G., Gouterman, M., Gallery, J. and Callis, J. (1993), Video Luminescent Barometry: The Induction Period, AIAA Paper 93-0179.

Upchurch, B. T., Oglesby, D. M., and West, J. P. (1998), New PSP developments at NASA Langley Research Center — Low temperature PSP, Proceeding of the Sixth Annual Pressure Sensitive Paint Workshop, The Boeing Company, Seattle, Washington, October 6-8, 10-1 to 10-24.

Verhaagen, N. G., Jenkins, L. N., Kern, S. B., and Washburn, A. E. (1995), A study of the vortex flow over a 76/40 deg double-delta wing, AIAA paper 95-0650.

Volan, A. and Alati, L. (1991), A New Optical Pressure Measurement System, Proc. 14th Int. Cong. Instrumentation in Aerospace Simulation Facilities (ICIASF), Institute of Electrical and Electronics Engineers, New York, pp. 10-16.

Weaver, W. L., Jordan, J. D., Dale, G. A., and Navarra, K. R. (1999), Data analysis methods for the development and deployment of pressure sensitive paints, AIAA Paper 99-0565.

Winslow, N. A., Carroll, B. F. and Setzer, F. M. (1996), Frequency Response of Pressure Sensitive Paints, AIAA Paper 96-1967.

Wong, K. W. (1980) Basic mathematics of photogrammetry, Chapter 2, *Manual of Photogrammetry*, 4th Edition, (C.C. Slama, editor), American Society of Photogrammetry, Falls Church, Virginia, 37-101.

Table I Sensitivity Coefficients and Elemental Errors

	Variable α_i	Sensitivity Coefficient S_i	Elemental Variance $var(\alpha_i)$	Physical Origin
1	$D_t(\Delta t)$	$\delta = 1 + \frac{A(T)}{B(T)}\frac{P_{ref}}{P}$	$[(\partial V/\partial t)(\Delta t)/V]^2$	Temporal variation in luminescence due to photodegradation and surface contamination
2	$D_x(\Delta x)$	δ	$[(\partial V/\partial x)^2\sigma_x^2 + (\partial V/\partial y)^2\sigma_y^2]V^{-2}$	Image registration error for correcting luminescence variation due to model motion
3	$D_{I0}(\Delta t)$	δ	$[(\partial I_0/\partial t)(\Delta t)/I_{0ref}]^2$	Temporal variation in illumination
4	V_{ref}	δ	$1/n_{pe\,ref}$	CCD camera noise
5	V	$-\delta$	$1/n_{pe}$	CCD camera noise
6	$D_c/D_{c\,ref}$	δ	$[R_2/(R_1+R_2)]^2(\Delta R_1/R_1)^2$	Change in camera performance parameters due to model motion
7	$D_f/D_{f\,ref}$	δ	$var(D_f/D_{f\,ref})$	Illumination spectral variability and filter spectral leaking
8	h/h_{ref}	δ	$[(\partial h/\partial x)^2\sigma_x^2 + (\partial h/\partial y)^2\sigma_y^2]h_{ref}^{-2}$	Image registration error for correcting thickness variation due to model motion
9	c/c_{ref}	δ	$[(\partial c/\partial x)^2\sigma_x^2 + (\partial c/\partial y)^2\sigma_y^2]c_{ref}^{-2}$	Image registration error for correcting concentration variation due to model motion
10	I_0/I_{0ref}	δ	$(I_{0ref})^{-2}\lvert(\nabla I_0)\cdot(\Delta X)\rvert^2$	Spatial variation in illumination due to model motion
11	P_{ref}	1	$var(P)$	Error in measurement of reference pressure
12	T	$-\frac{T}{B(T)}[B'(T)+A'(T)\frac{P_{ref}}{P}]$	$var(T)$	Error in temperature measurement
13	A	$1-\delta$	$var(A)$	Paint calibration error
14	B	-1	$var(B)$	Paint calibration error
15	Pressure mapping	1	$(\partial P/\partial x)^2\sigma_x^2 + (\partial P/\partial y)^2\sigma_y^2$ and $\lvert(\nabla P)_{surf}\cdot(\Delta X)_{surf}\rvert^2$	Errors in camera calibration and pressure mapping on a surface of a rigid body

Note: σ_x and σ_y are the standard deviations of least-square estimation in the image registration or camera calibration.

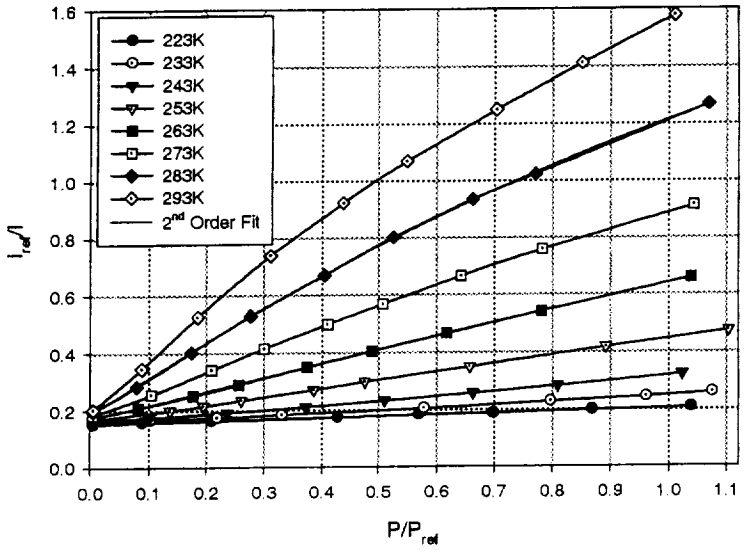

(a)

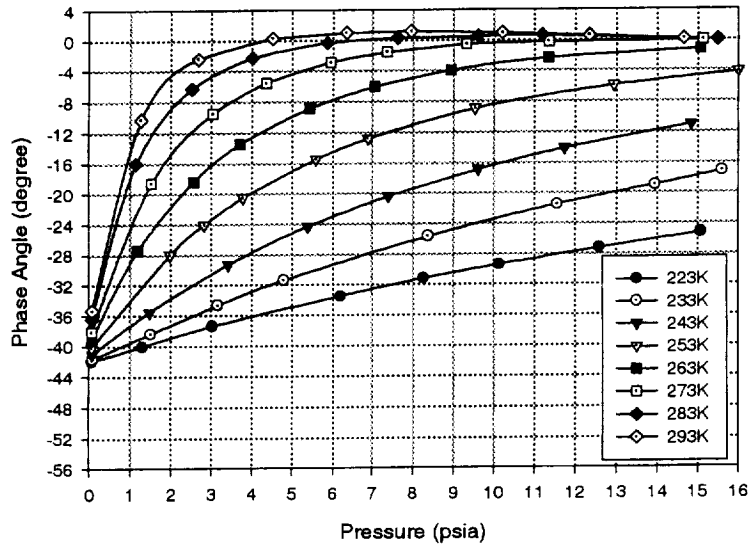

(b)

Figure 1. Calibration results for PtTFPP adsorbed onto a tape made of a polymer/ceramic composite composed of aluminum oxide particles and about 25% volume of a poly(acrylic) binder. (a) Stern-Volmer plot, (b) Phase plot when sine-wave modulation is at 6kHz. The reference pressure is 14.5psi and reference temperature is 277K.

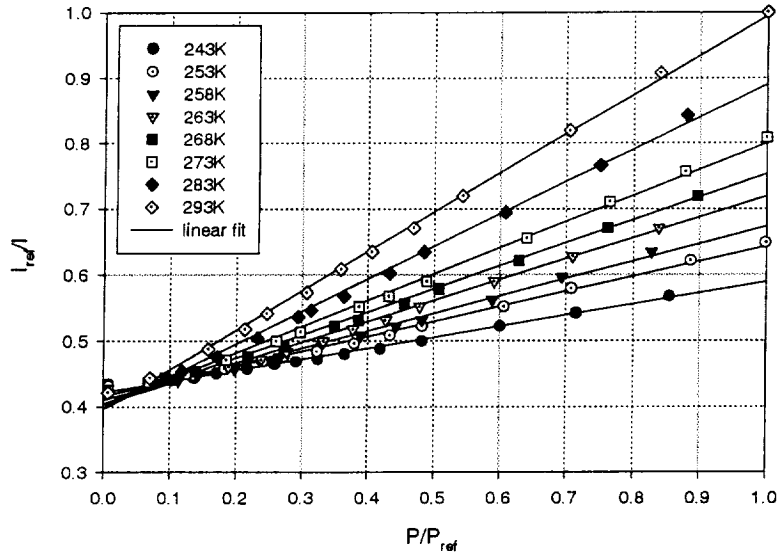

(a)

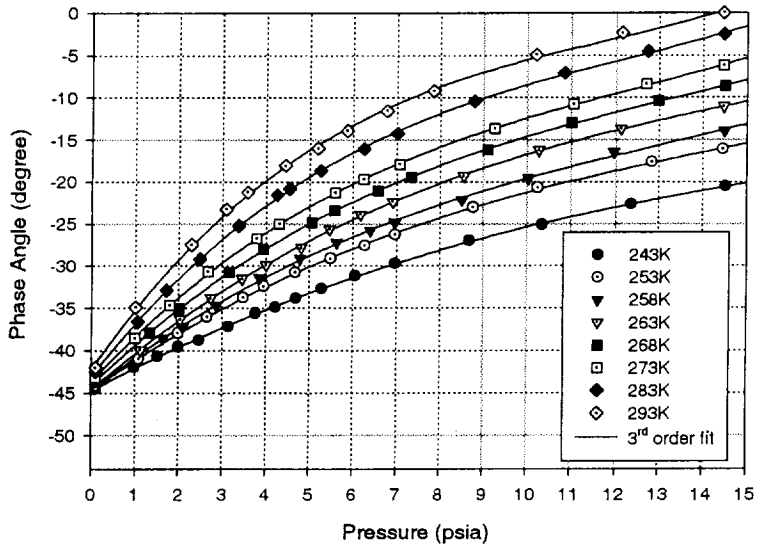

(b)

Figure 2. Calibration results for Bathophen Ruthenium Chloride in RTV 110 and Silica Gel. (a) Stern-Volmer plot, (b) Phase plot when sine-wave modulation is at 80kHz. The reference pressure is 14.5psi and reference temperature is 293K.

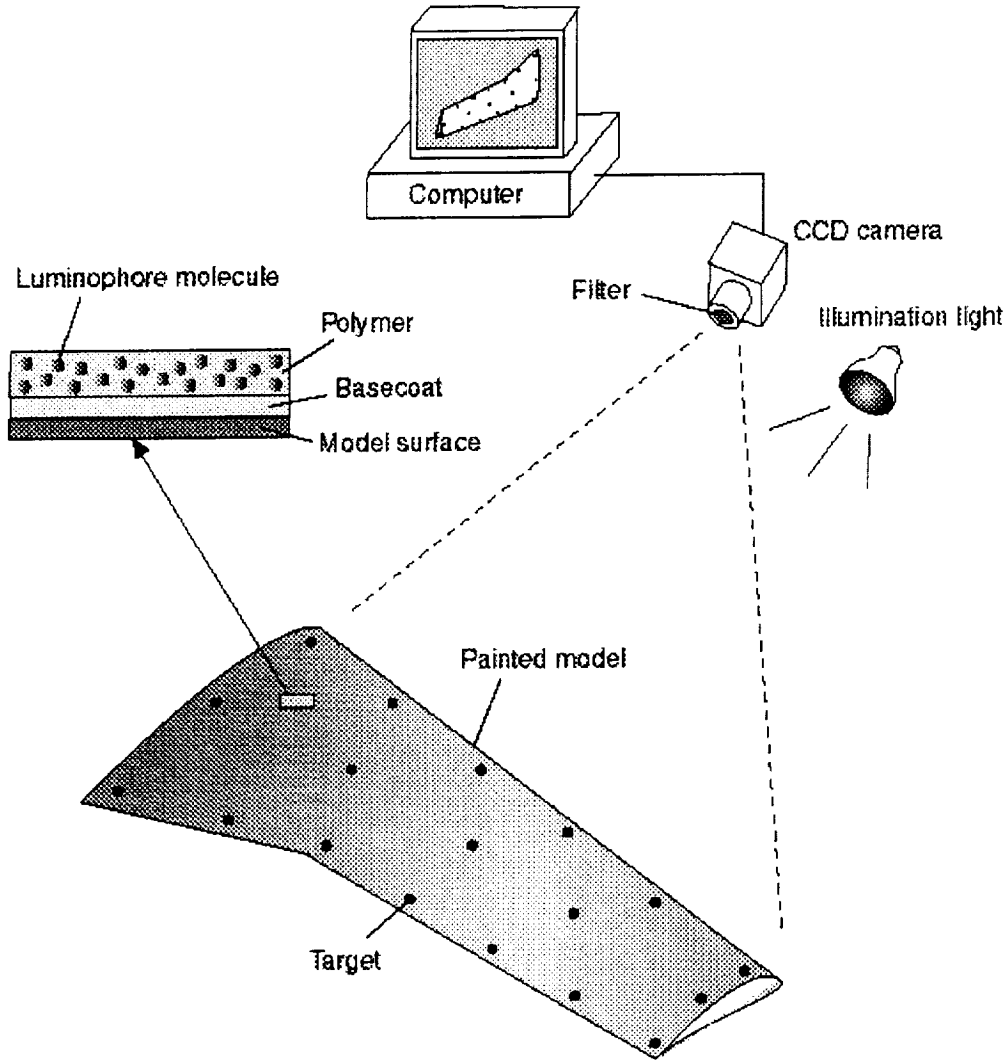

Figure 3. A CCD camera system for PSP

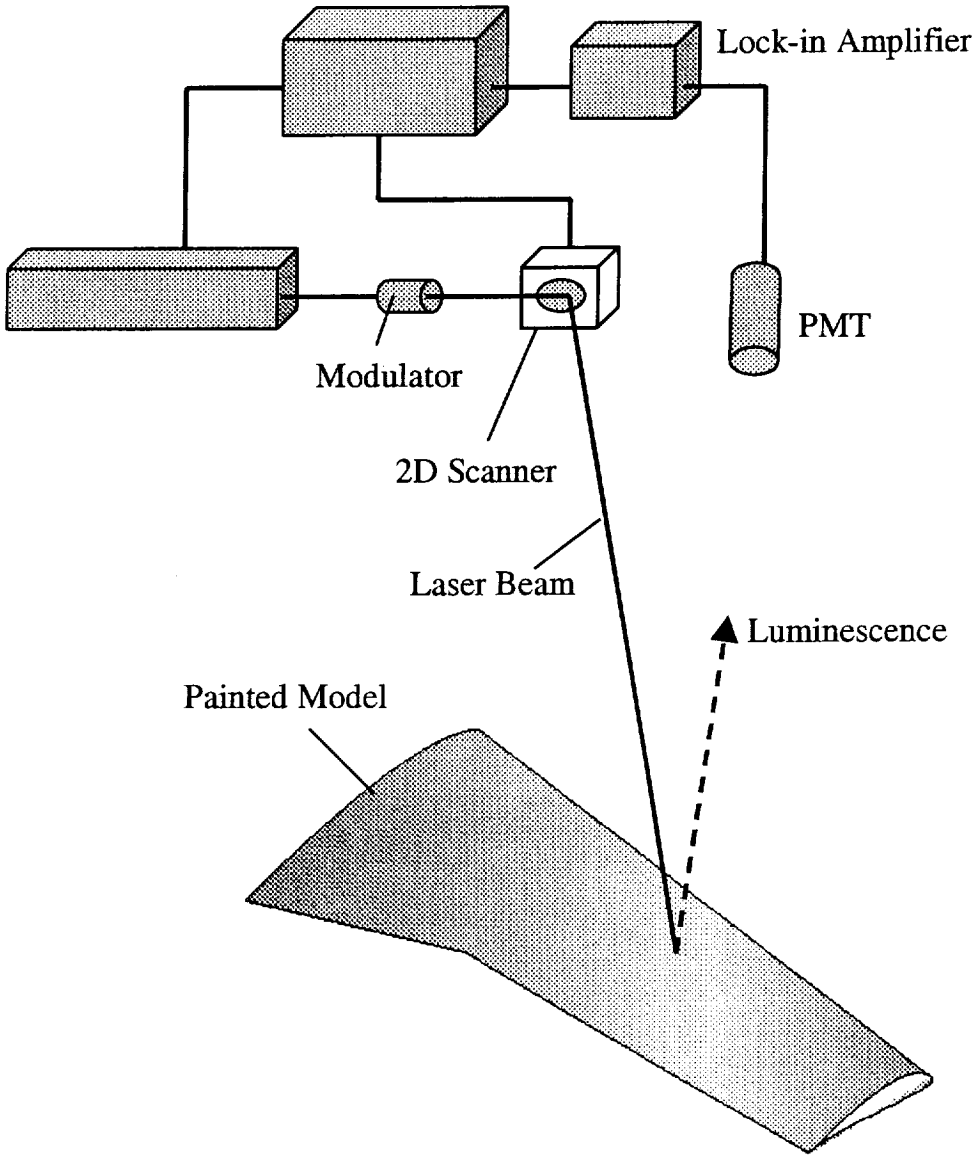

Figure 4. A generic laser scanning lifetime system

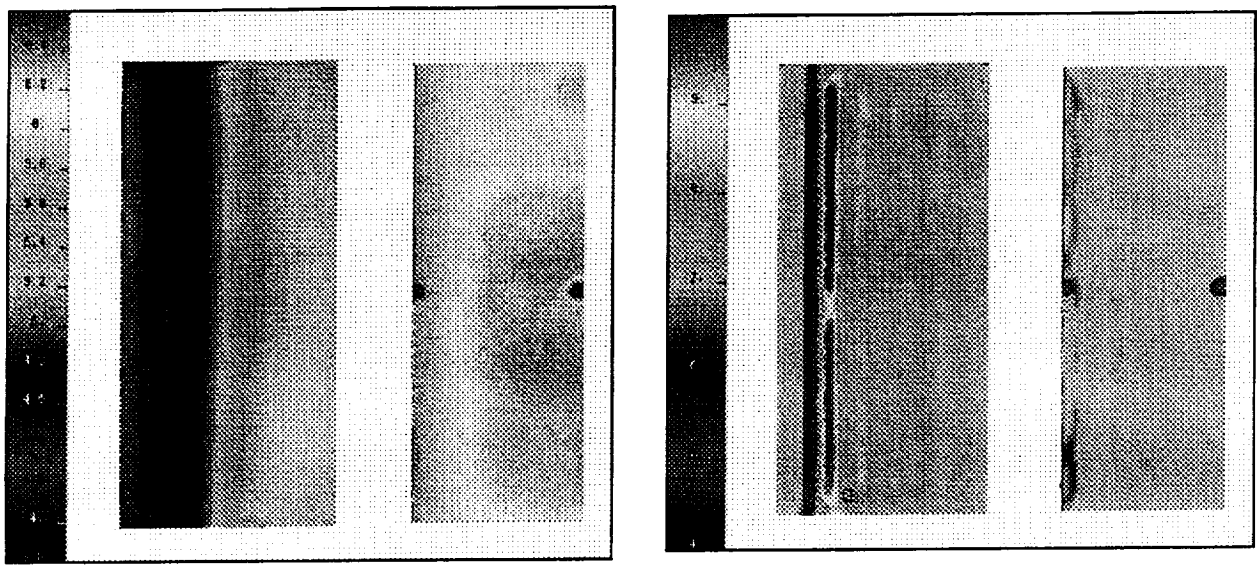

(a) (b)

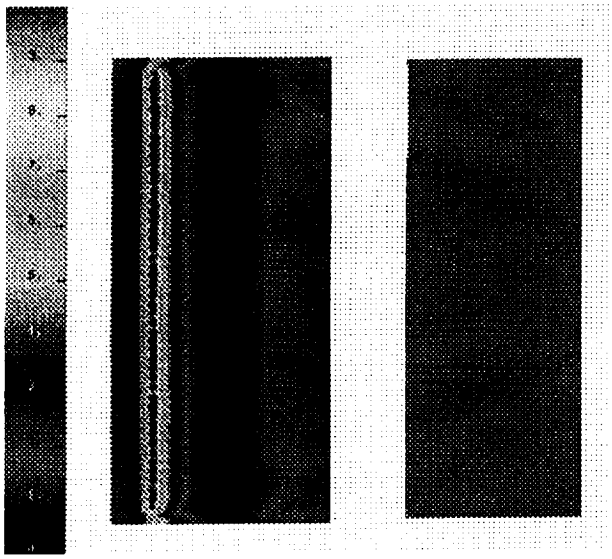

Figure 5. PSP images of boundary layer control using blowing from a recessed aft facing step. (a) no blowing at Mach 1.3, (b) maximum blowing mass flow at Mach 1.3, (c) maximum blowing mass flow at Mach 2.5.

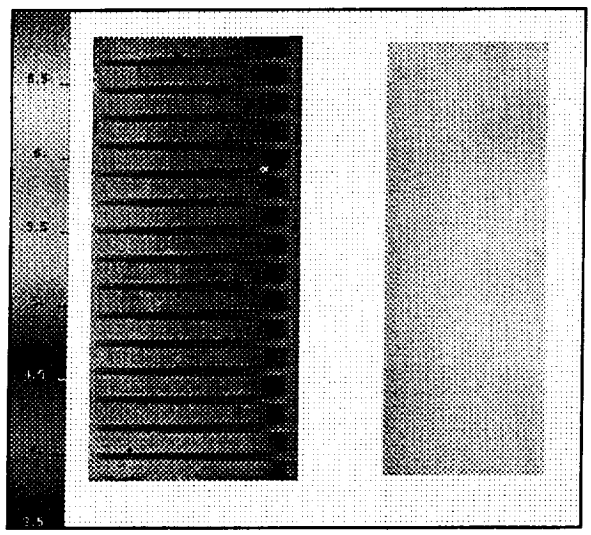

(a)

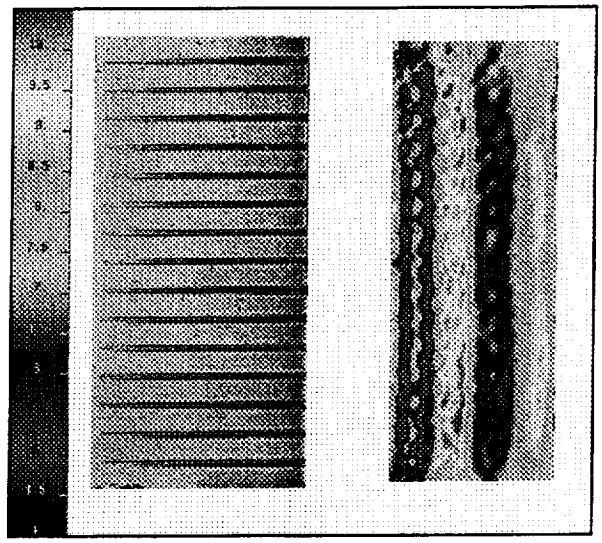

(b)

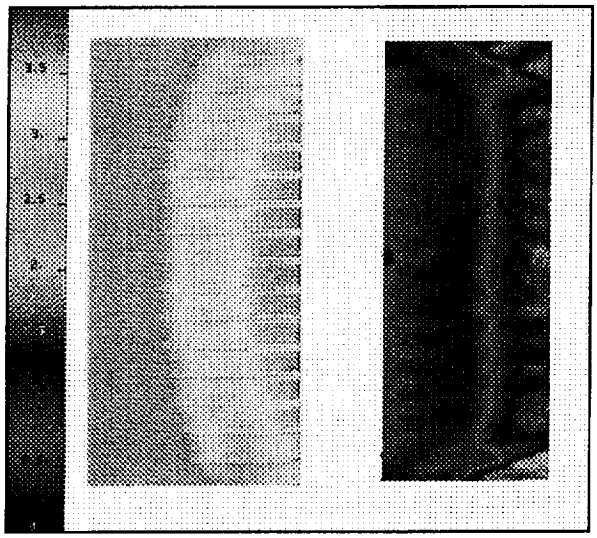

(c)

Figure 6. PSP images of boundary layer control using blowing from a raised insertion plane. (a) no blowing at Mach 1.3, (b) maximum blowing mass flow at Mach 1.3, (c) maximum blowing mass flow at Mach 2.5.

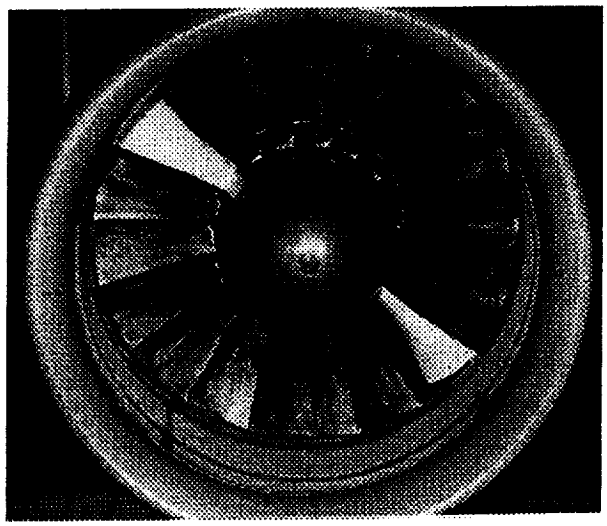

Figure 7. PSP and TSP painted blades mounted in ultra-high bypass ratio fan rig.

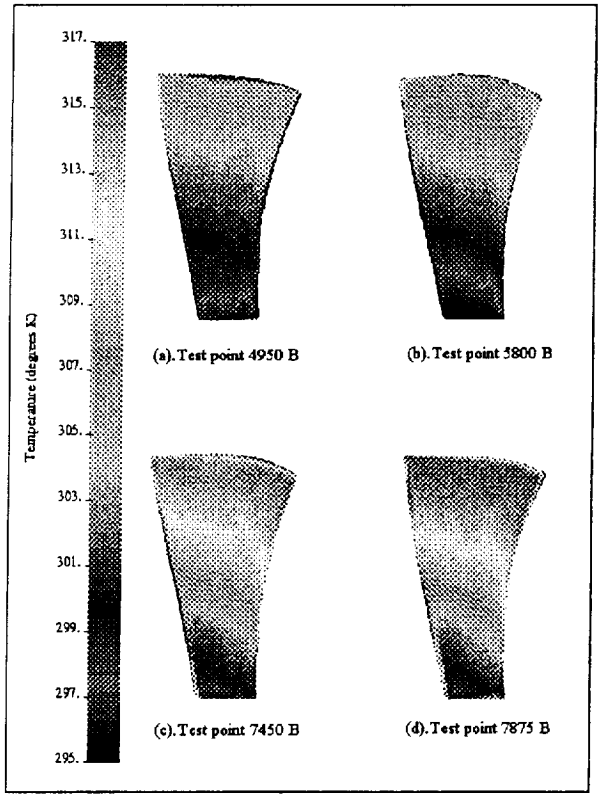

Figure 8. Temperature profiles of the TSP blade at four rig speeds.

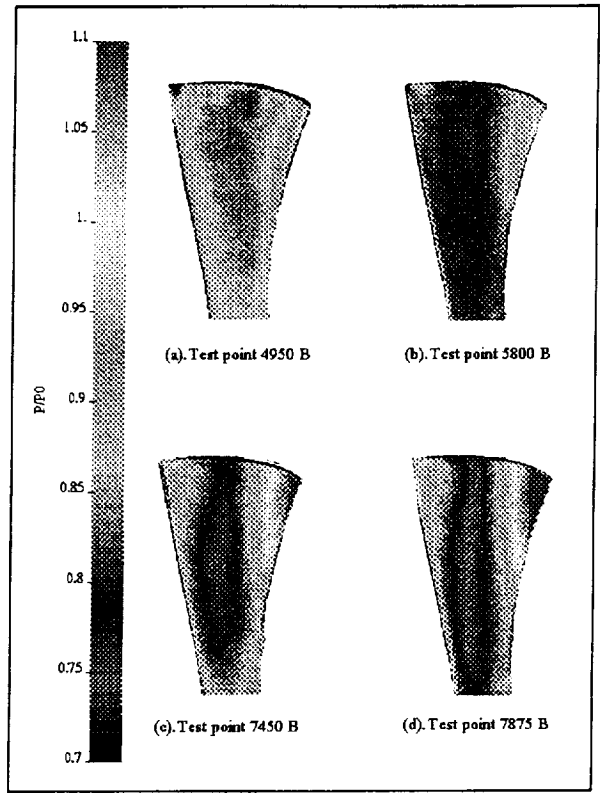

Figure 9. Normalized pressure profiles of the temperature corrected PSP blade at four rig speeds

National Aeronautics and
Space Administration
Lewis Research Center
Cleveland, OH 44135-3191

Reply to Attn of: 0620

NASA Center for AeroSpace Information
7121 Standard Drive
Hanover, MD 21076

Enclosed are copies of NASA Lewis and/or contractor authored open literature reprints and conference preprints not printed as Technical Memorandums.

If you have any questions about any of these papers, or changes regarding this distribution, please contact the Publishing Services Coordination Office at (216) 433-5810 or FAX (216) 433-5783. Mail can be addressed to NASA Lewis Research Center, 21000 Brookpark Road, Mail Stop 21-8, Cleveland, Ohio 44135.

Sue Butts
Technical Publications Manager

Enclosures
1. Reports